1.B:2.B

Nuclear Physics **A348** (1980) 388–428

MESON–BARYON DYNAMICS AND THE $pp \leftrightarrow d\pi^+$ REACTION (I). Total and differential cross sections*

O.V. MAXWELL, W. WEISE** and M. BRACK

Institute of Theoretical Physics, University of Regensburg, D-8400 Regensburg, W. Germany

Received 17 December 1979
(Revised 29 April 1980)

Abstract: We have obtained σ_{tot} and $d\sigma/d\Omega$ for $\pi^+ d \leftrightarrow pp$ using the most recent version of the Paris NN interaction. The model consists of the impulse approximation, p-wave pion and rho-meson rescattering following Δ_{33} excitation, and s-wave rescattering constructed from the Koltun–Reitan lagrangian plus off-shell extrapolations. The rho mass distribution is described using the square of the Paris f_-^1 helicity amplitude, and monopole form factors have been included in the internal πNN and $\pi N\Delta$ vertices. Recoil corrections to the impulse approximation are also considered and turn out to be important. Results are obtained with the Paris and Reid interactions as a function of the $\rho N\Delta$ coupling constant, $\alpha_\rho = f_\rho^*/f_\rho$, and cutoffs Λ_π (varied between 1.7 and 2.0 and between 1.0 and 1.4 GeV respectively). Reasonable agreement with the experimental σ_{tot} can be obtained with either potential within the parameter ranges considered. Results for $d\sigma/d\Omega$, parametrized in the form $d\sigma/d\Omega = (1/32\pi)(\gamma_0 + \gamma_2 \cos^2\theta + \gamma_4 \cos^4\theta + \cdots)$, reveal that high partial waves ($l_{pp} > 3$) play a significant role, particularly in γ_4. This coefficient is particularly sensitive to α_ρ and may ultimately provide a constraint on that parameter.

1. Introduction

Pion-induced disintegration of the deuteron, $\pi^+ d \to pp$, and the inverse process have recently generated considerable theoretical and experimental interest. Theoretically, this interest has a dual motivation. On the one hand, these reactions are simple enough to be treated within the framework of detailed microscopic models and as such, provide a significant test of current understanding of elementary πN processes, particularly the off-shell πN interaction and the $\rho N\Delta$ vertex. On the other hand, it is hoped that a good understanding of the simple processes will provide the basis for analyses of more complicated meson-nuclear processes. Some progress has already been made in this direction [1–3]).

Experimentally, data for the total absorption cross section and the unpolarized part of the differential cross section have been obtained for c.m. momenta from threshold up to about 2.7 pion masses. Several compilations of these data now exist, which combine results from both the π-production and absorption reactions [4–8]).

* Work supported in part by German Bundesministerium für Forschung und Technologie.
** Also at CERN, Geneva.

The data for the total cross section exhibit a resonant structure, with a peak of about 12 mb near a c.m. momentum of about 1.6 pion masses. Recently, the empirical data have been extended so as to include the polarization parameters [8–9]).

Several theoretical studies of pionic deuteron disintegration have been carried out, based on rather different approaches. Alberg *et al.* [10]) employ a field-theoretic formalism which, however, omits two-pion exchange processes. Moreover, it does not predict the correct static limit for the one pion exchange interaction, a most peculiar feature.

A second approach, that of Niskanen [11]), is based on a coupled channels formalism that permits multiple rescattering diagrams to be included to all orders. In principle, this is probably the best approach, but it is unfortunately fraught with complexities of sufficient magnitude to make it necessary to handle each partial wave contribution to the T-matrix separately. This limits somewhat the number of partial waves that can be handled within a feasible calculation. Although not significant for the total cross section, such a limitation may be important for the differential cross section, which we have found is significantly influenced by the inclusion of high pp partial waves. Moreover, it is not at all a trivial procedure to avoid double counting within the coupled-channels formalism when the rescattered pions are supplemented with other mesons.

As an alternative to these approaches, Brack, Riska and Weise [12]) (BRW) proposed a model which is relatively simple and at the same time incorporates the major dynamical features thought to be relevant in pionic deuteron disintegration. It is based on the three T-matrix contributions depicted in fig. 1: the impulse approximation (IA), a p-wave rescattering mechanism involving the excitation of an intermediate Δ_{33} resonance followed by either one-pion exchange (OPE) or the isovector-vector part of two-pion exchange [$2\pi(1^-)$ exchange], and an s-wave rescattering mechanism based upon the phenomenological, zero-range lagrangian of Koltun and Reitan [13]) (KR). The rescattering contributions are necessitated by the kinematics of the reaction which require a large momentum transfer between the two nucleons in order to conserve both energy and momentum. This is difficult to achieve with the impulse approximation alone, and in fact, the impulse approximation does not even yield the right order of magnitude for the cross section. Inclusion of the p-wave rescattering mechanism not only yields the right order of magnitude but also reproduces the observed resonance structure, which is clearly associated with the intermediate Δ_{33} resonance. The s-wave rescattering mechanism is necessary to obtain the low-momentum part of the cross section correctly.

BRW employed this model in conjunction with the Reid potential to compute the total cross section for $\pi^+ \mathrm{d} \to \mathrm{pp}$. Using reasonable values for α_ρ, the ratio of the $\rho \mathrm{N}\Delta$ and $\pi \mathrm{N}\Delta$ couplings, and Λ_π, the cut-off in the πNN form factor, they obtained a good fit to the empirical data. Subsequently, Chai and Riska [14]), utilizing essentially the same model, have carried out calculations of the differential cross section and polarization parameters for $\mathrm{pp} \to \pi^+ \mathrm{d}$.

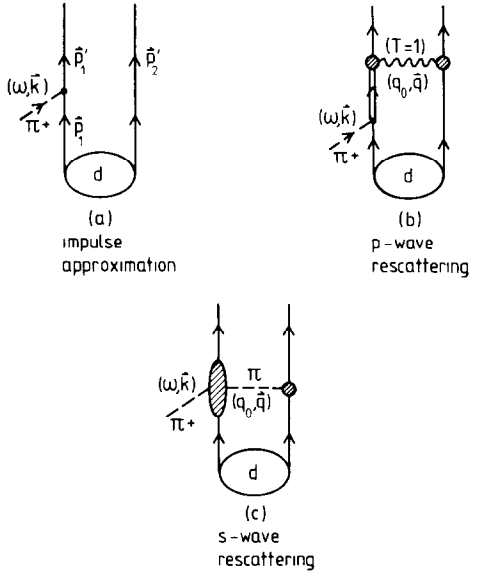

Fig. 1. Contributions to the T-matrix as discussed in the text. The wavy line in diagram (b) represents OPE plus $2\pi(1^-)$ exchange (see text for notation); the circular shaded areas in diagrams (b) and (c) represent the extended structures of the πNN and πNΔ vertices; the elliptical shaded area in diagram (c) represents the effective $\pi\pi$NN s-wave vertex.

The present work is based upon the BRW model but modifies it in several respects with the idea of improving the representation of the physics underlying the relevant processes. These modifications may be summarized as follows:

(a) We have improved the description of the Δ_{33} resonance in ref. [12]) by replacing the BRW form for the Δ_{33} propagator by a form that preserves the relativistic result for the resonant πN scattering amplitude in the (3, 3) channel. In addition, the effect of crossed Born terms on the effective πNΔ coupling and the Δ_{33} width have been examined in some detail.

(b) The model for the s-wave rescattering contribution has been supplemented with form factors that permit the on-shell, phenomenological parameters appearing in the KR lagrangian to be extrapolated off-shell in a simple manner. We have further improved the s-wave rescattering model by utilizing more recent values for the πN scattering lengths to fix the parameters on-shell.

(c) The combination of helicity amplitudes in the $2\pi(1^-)$ exchange part of the p-wave rescattering mechansim has been modified so as to include second-order rescattering terms.

(d) We have included approximate recoil corrections, based upon both the pseudoscalar and pseudovector forms for the πNN vertex, in the impulse approximation matrix element. These corrections have a significant effect both on the total and the differential cross section.

(e) Finally, we have studied the effect of distortions of the pion-wave induced by elastic πd scattering on the πd disintegration process [15,16]).

With these modifications we have employed the BRW model to compute the total cross section for the pion absorption process and the unpolarized differential cross section, parametrized in the usual power series form

$$\frac{d\sigma}{d\Omega} = \frac{1}{32\pi}(\gamma_0 + \gamma_2 \cos^2\theta_{c.m.} + \gamma_4 \cos^4\theta_{c.m.} + \cdots), \tag{1.1}$$

for the pion production process. Our main purpose in these calculations has been to uncover the dependence of the cross section on the various features of the model utilized. Thus, we have carried out a spectrum of calculations spanning a range of choices for the relevant parameters. In place of the phenomenological Reid potential employed in ref. [12]) to represent the deuteron wave function and the NN interaction in the relative pp state, we have adopted the dispersion-theoretic Paris potential [17]) which rests on a solid theoretic foundation and thus, is more appropriate for use in calculations based on microscopic models. For comparison purposes a number of results have also been obtained with the Reid potential.

Following a brief summary of the relevant cross section formulae in sect. 2, the extended BRW model is described in sect. 3, with particular attention paid to the present modifications. Sect. 4 contains numerical results for both total and differential cross sections together with an interpretation of these. Finally, the last section is devoted to discussion and conclusions.

2. The cross section for $\pi^+ d \to pp$

It is most convenient to evaluate the pion absorption cross section in the laboratory frame, where the deuteron is at rest and the incoming pion can be represented by a plane wave of momentum $\boldsymbol{k}$ and energy $\omega = \sqrt{k^2 + m_\pi^2}$ (m_π is the pion rest mass). In this frame,

$$d\sigma = \frac{1}{2k}\frac{d^3p}{(2\pi)^3}\frac{d^3P}{(2\pi)^3}(2\pi)^4\delta^3(\boldsymbol{P}-\boldsymbol{k})\delta(E_1+E_2-2M+B_d-\omega)\frac{1}{3}\sum|T_{fi}|^2, \tag{2.1}$$

where $\boldsymbol{P}$ and $\boldsymbol{p}$ are the c.m. and relative momenta in the outgoing pp state, E_1 and E_2 are the (relativistic) energies of the outgoing protons, M is the nucleon mass, B_d the deuteron binding energy, and T_{fi} the matrix element of the T-matrix between the initial and final nucleon states. The sum here is to be carried out over the allowed spin states of the deuteron and the outgoing pp state (the factor $\frac{1}{3}$ ensures that the initial spin states are averaged over).

Momentum and energy conservation constrain the relative momentum p to a function of k and θ_l, the angle subtended by $\hat{\boldsymbol{p}}$ relative to $\hat{\boldsymbol{k}}$ in the laboratory frame. In

particular, neglecting the deuteron binding energy,

$$p \cong \sqrt{\frac{M\omega + \frac{1}{4}m_\pi^2}{1 - \varepsilon \cos^2 \theta_l}} \tag{2.2}$$

with $\varepsilon \equiv k^2/E^2$, E denoting the total energy in the laboratory frame. Inserting this into (2.1) and performing the integrals over $\boldsymbol{P}$ and p yields the differential cross section in the laboratory frame,

$$\frac{\mathrm{d}\sigma}{\mathrm{d}\Omega_{\mathrm{lab}}} \cong \frac{p(M + \frac{1}{2}\omega)}{(4\pi)^2 k} \frac{1 - 4(p/E)^2 \varepsilon \cos^2 \theta_l}{1 - \varepsilon \cos^2 \theta_l} \frac{1}{3} \sum_{\mathrm{i,f}} |T_{\mathrm{fi}}|^2 , \tag{2.3}$$

where Ω_{lab} is the solid angle corresponding to θ_l, and we have approximated $E \cong \omega + 2M$. The corresponding c.m. quantity is easily derived from (2.3) using the relationship between θ_l and the c.m. scattering angle, $\theta_{\mathrm{c.m.}}$,

$$\cos^2 \theta_l = \cos^2 \theta_{\mathrm{c.m.}} / (1 - \varepsilon \sin^2 \theta_{\mathrm{c.m.}}) . \tag{2.4}$$

We obtain

$$\frac{\mathrm{d}\sigma}{\mathrm{d}\Omega_{\mathrm{c.m.}}} = \frac{\mathrm{d}\sigma}{\mathrm{d}\Omega_{\mathrm{lab}}} \frac{\mathrm{d}\Omega_{\mathrm{lab}}}{\mathrm{d}\Omega_{\mathrm{c.m.}}} = \frac{\mathrm{d}\sigma}{\mathrm{d}\Omega_{\mathrm{lab}}} \frac{\cos \theta_l}{\cos \theta_{\mathrm{c.m.}}} (1 - \varepsilon \cos^2 \theta_l) . \tag{2.5}$$

Since $\varepsilon \leqslant 0.02$ for the momenta of interest, eqs. (2.2)–(2.5) can all be expanded in powers of ε. Thus, we arrive at the simple power series expression for $\mathrm{d}\sigma/\mathrm{d}\Omega_{\mathrm{c.m.}}$, eq. (1.1). The total cross section is just

$$\sigma_{\pi \mathrm{d} \to \mathrm{pp}} = \frac{1}{2} \int \mathrm{d}\Omega \frac{\mathrm{d}\sigma}{\mathrm{d}\Omega} , \tag{2.6}$$

the factor of $\frac{1}{2}$ arising from the indistinguishability of the final protons.

The empirical cross sections are usually given as functions of the πd c.m. momentum, rather than the laboratory momentum. Moreover, the p-wave rescattering process involves the momentum in the c.m. of the π-nucleon system. For quantitative calculations, it is necessary that the relativistic relations connecting these three momenta be fully preserved. Since this point has not been adequately appreciated in the literature, particularly in ref. [12]), we have devoted an appendix (appendix A) to a simple derivation of the relevant relations.

3. Contributions to the T-matrix

The model for the total T-matrix comprises the three contributions depicted in fig. 1, i.e., the impulse approximation (IA), the p-wave rescattering term, and the s-wave rescattering term:

$$T_{\mathrm{fi}} = \langle \psi_{\mathrm{pp}} | \hat{M}_{\mathrm{IA}} + \hat{M}_{\mathrm{p}} + \hat{M}_{\mathrm{s}} | \psi_{\mathrm{d}} \rangle . \tag{3.1}$$

In this section we discuss each of these three contributions in some detail.

3.1. THE IMPULSE APPROXIMATION

The IA contribution is obtained from the non-relativistic reduction of the pseudoscalar or pseudovector coupling πNN lagrangian acting between plane wave Dirac spinors. For absorption on the ith nucleon ($i = 1, 2$), this is given by

$$L_{\pi\mathrm{NN}} = -\frac{f}{m_\pi}\boldsymbol{\sigma}_i \cdot \left[\left(1-\alpha\frac{\omega}{M}\right)\boldsymbol{k} - \beta\frac{\omega}{M}\tfrac{1}{2}(\boldsymbol{p}_i+\boldsymbol{p}_i')\right]\tau_{i\lambda}\pi_\lambda\,, \tag{3.2}$$

where $\boldsymbol{k}$ and ω are the pion lab momentum and energy, $\boldsymbol{\sigma}_i$ and $\tau_{i\lambda}$ are the spin and isospin matrices, π_λ is the pion field, and $\boldsymbol{p}_i$ and $\boldsymbol{p}_i'$ are the incoming and outgoing nucleon momenta. The parameters α and β here reflect the ambiguity inherent in the πNN vertex for off-shell nucleons. They assume fixed values once the form of the vertex is specified. In particular, for psedudoscalar coupling (PS) we have

$$\alpha = \tfrac{1}{4}\,, \qquad \beta = \tfrac{1}{2} \tag{3.3}$$

and for pseudovector coupling (PV),

$$\alpha = 0\,, \qquad \beta = 1\,. \tag{3.4}$$

In ref. [12]) the PV form was employed with the recoil term neglected ($\beta = 0$). This gives for the corresponding T-matrix contribution, after specializing to the case of an incoming π^+,

$$\hat{M}_{\mathrm{IA}}(\boldsymbol{k}, \boldsymbol{r}) = -\frac{f}{m_\pi}[\mathrm{e}^{i\boldsymbol{k}\cdot\boldsymbol{r}/2}(\boldsymbol{\sigma}_1\cdot\boldsymbol{k})\sqrt{2}\tau_{1+} + \mathrm{e}^{-i\boldsymbol{k}\cdot\boldsymbol{r}/2}(\boldsymbol{\sigma}_2\cdot\boldsymbol{k})\sqrt{2}\tau_{2+}]\,, \tag{3.5}$$

where the two terms arise from pion absorption on the left and right nucleon lines respectively.

The recoil terms in (3.2) are expected to be small for $\omega \ll M$ and $k > 0$. Near threshold, however, where $k \sim 0$, they are the dominant contribution to $L_{\pi\mathrm{NN}}$ and cannot be neglected. Even for large k, they may provide a significant contribution to the T-matrix, since ω is an appreciable fraction of M, and the momenta $\boldsymbol{p}_i$ and $\boldsymbol{p}_i'$ must be treated as derivative operators when evaluating coordinate space matrix elements. In general, it is difficult to assess the importance of these recoil terms since this would involve differentiation of both the initial and final-state nucleon wavefunctions. However, if we neglect correlations in the final state[†], we find

$$\tfrac{1}{2}(\boldsymbol{p}_i+\boldsymbol{p}_i') = \pm\boldsymbol{p}\,, \tag{3.6}$$

where $\boldsymbol{p}$ is the relative momentum in the outgoing pp state and the + or − is chosen according to whether $i = 1$ or 2. The significance of this simple relation is that $\boldsymbol{p}$ operates only on the final-state wave function.

[†] In fact, it has been shown in ref. [12]) that final-state pp correlations are not of extreme importance, so they may be safely neglected when evaluating recoil corrections. Such conclusions can also be drawn by comparison with the calculation of Shimizu *et al.* [34]), who have included final-state correlations.

Using (3.6) in (3.2), we obtain for the IA contribution to the T-matrix, in place of (3.5),

$$\hat{M}_{\mathrm{IA}}(\boldsymbol{k}, \boldsymbol{r}) = -\frac{f}{m_\pi}\left\{ \mathrm{e}^{i\boldsymbol{k}\cdot\boldsymbol{r}/2}\boldsymbol{\sigma}_1 \cdot \left[\left(1-\alpha\frac{\omega}{M}\right)\boldsymbol{k} + \beta\frac{\omega}{M}\boldsymbol{p}\right]\sqrt{2}\tau_{1+} \right.$$
$$\left. + \mathrm{e}^{-i\boldsymbol{k}\cdot\boldsymbol{r}/2}\boldsymbol{\sigma}_2 \cdot \left[\left(1-\alpha\frac{\omega}{M}\right)\boldsymbol{k} - \beta\frac{\omega}{M}\boldsymbol{p}\right]\sqrt{2}\tau_{2+}\right\}. \tag{3.7}$$

It should be emphasized that this is only an approximate relation, not only because final-state correlations have been neglected in (3.6), but also because the non-relativistic form for $L_{\pi\mathrm{NN}}$, eq. (3.2), is strictly valid only for plane wave states; it is not at all clear how (3.2) would be altered if a relativistic deuteron wave function were employed in place of the plane wave Dirac spinor used to obtain that relation. Nevertheless, we believe that eq. (3.7) can yield at least some indication of the influence of recoil corrections on the πd disintegration cross section.

3.2. p-WAVE RESCATTERING

As depicted in fig. 1b, the p-wave rescattering mechanism involves the excitation of a Δ_{33} resonance, which subsequently decays through emission of either a single off-shell pion or a pair of pions that transfer large momenta to the other nucleon. The analogous process with an intermediate nucleon line in place of the resonance is also possible, but since this is already counted in the IA contribution to the T-matrix through inclusion of initial- and final-state correlations, it has to be omitted here. By virtue of its isospin structure, the crossed diagram constructed by interchanging the two $\pi\mathrm{N}\Delta$ vertices in the diagram shown is identically zero. Of course, the incident pion in fig. 1b may be attached to either nucleon line, and these two contributions must be summed coherently.

In position space the p-wave rescattering contribution to the T-matrix is

$$\hat{M}_{\mathrm{p}}(\boldsymbol{k}_{\pi\mathrm{N}}, \boldsymbol{r}) = \frac{f^*_{\mathrm{eff}}(s)}{m_\pi} D_\Delta(s, k_{\pi\mathrm{N}})[\mathrm{e}^{i\boldsymbol{k}\cdot\boldsymbol{r}/2}\tilde{V}_{12}(\boldsymbol{r})(\boldsymbol{S}_1^+ \cdot \boldsymbol{k}_{\pi\mathrm{N}})T_{1+}^+$$
$$+ \mathrm{e}^{-i\boldsymbol{k}\cdot\boldsymbol{r}/2}\tilde{V}_{21}(\boldsymbol{r})(\boldsymbol{S}_2^+ \cdot \boldsymbol{k}_{\pi\mathrm{N}})T_{2+}^+], \tag{3.8}$$

where $\boldsymbol{k}_{\pi\mathrm{N}}$ is the πN c.m. momentum, f^*_{eff} is the effective coupling at the external $\Delta\mathrm{N}\pi$ vertex[†], D_Δ is the Δ_{33} propagator, $\tilde{V}_{12}$ is the effective NΔ-NN transition potential with the Δ on the l.h.s., $\boldsymbol{S}$ and $\boldsymbol{T}$ are the transition spin and isospin operators, and $\sqrt{s}$ is the total πN c.m. energy. We employ the form

$$D_\Delta^{-1} = M_\Delta - \sqrt{s} - \tfrac{1}{2}i\Gamma_\Delta(s, k_{\pi\mathrm{N}}) \tag{3.9}$$

[†] No t-channel cutoff factor is to be included in the external $\pi\mathrm{N}\Delta$ vertex, since the external pion is on-shell. Proper use of $k_{\pi\mathrm{N}}$ in the $\pi\mathrm{N}\Delta$ vertex increases σ_{tot} by about 2 mb as compared to the BRW result.

for the Δ_{33} propagator, where $M_\Delta = 1232$ MeV and Γ_Δ are the Δ_{33} mass and width. For the Δ_{33} width, we adopt the form

$$\Gamma_\Delta = \frac{2}{3}\frac{f^{*2}_{\rm eff}(s)}{4\pi}\frac{k^3_{\pi N}}{m^2_\pi}. \tag{3.10}$$

To account for relativistic corrections in the Δ_{33} propagator, we write

$$f^{*2}_{\rm eff}(s) = f^{*2}(s)\frac{2M_\Delta}{M_\Delta + \sqrt{s}}. \tag{3.11}$$

Several choices are possible for $f^*(s)$. The simplest one assumes f^* to be independent of s and relates it to the Chew-Low model [18]), i.e.

$$f^{*2}/4\pi = 0.32\,, \tag{3.12}$$

although the Δ-width comes out slightly too large at $s = M^2_\Delta$ in this case. A relativistic description of the Δ_{33} part of the πN c.m. amplitude† gives $f^{*2}/4\pi = 0.37\ (M_N/\sqrt{s})$. We shall adopt eq. (3.12) as a "standard" value, but discuss alternative choices in sect. 5.

The role of crossed Born terms in the πN c.m. amplitude in the 3, 3 channels requires additional discussion. We have already mentioned that the isolated crossed Born term in the p-wave rescattering amplitude should be omitted in order not to double count with two-nucleon correlations explicitly taken into account. On the other hand, diagrams of the type shown in fig. 4a also contribute and could simply be incorporated by multiplying $f^*_{\rm eff}$ by the appropriate u-channel form factor so as to treat the nucleon poles correctly. However, the diagram of fig. 4b, which is of the same order, also appears in the two-nucleon system, and partly cancels fig. 4a. In essence, it is not legitimate to include left-hand cut contributions to the p-wave rescattering amplitude unless one takes into account related two-body diagrams at the same time††. With such partial cancellations present (but not under complete control quantitatively), we prefer to omit u-channel cut corrections, as well as their two-body analogues and retain the simplest treatment, eqs. (3.8)–(3.12). The role of u-channel cut contributions to the Δ-width will be discussed separately in sect. 5.

A final comment concerns recoil corrections to the external $\pi N\Delta$ vertex appearing in eq. (3.8). The form employed there is the correct one as derived from the Rarita–Schwinger formalism in the πN c.m.s., where the isobar is at rest. In principle, recoil corrections due to nucleon motion can be obtained from the fully relativistic formalism [30]). Unfortunately, the Rarita–Schwinger description is not

† We are grateful to E. Oset for discussions on this point; see also ref. [28]).

†† This remark applies in particular to models which use the full empirical πN scattering amplitude in the rescattering diagram [16]) without considering further its underlying structure.

unique for an off-shell isobar so that any particular form of recoil corrections is difficult to justify†. We therefore use eq. (3.8) throughout.

In our model for the NΔ–NN transition potential, we include one- and two-pion exchange terms. Isospin conservation requires that the exchange be of isovector character; thus, the two-pion exchange terms must have the spin–isospin structure of the ρ-meson. This motivates the notation

$$\tilde{V}_{12}(\boldsymbol{r}) = V^{\pi}_{12}(\boldsymbol{r}) + V^{\rho}_{12}(\boldsymbol{r}), \tag{3.13}$$

where the terms on the right are the one-pion exchange (OPE) and isovector-vector two-pion exchange [$2\pi(1^-)$ exchange] pieces respectively.

3.2.1. One-pion exchange. The first term on the r.h.s. of eq. (3.13) is obtained from the usual, non-relativistic OPE interaction between two nucleons by just replacing one set of spin and isospin matrices by transition spin and isospin operators. In momentum space, this yields

$$V^{\pi}_{12}(\boldsymbol{q}) = \frac{f^*(q)f(q)}{m_\pi^2} \frac{\boldsymbol{S}_1 \cdot \boldsymbol{q}\boldsymbol{\sigma}_2 \cdot \boldsymbol{q}}{q_0^2 - \boldsymbol{q}^2 - m_\pi^2} \boldsymbol{T}_1 \cdot \boldsymbol{\tau}_2, \tag{3.14}$$

where $q = (q_0, \boldsymbol{q})$ is the 4-momentum transferred by the exchanged pion. In principle the evaluation of (3.8) with the Fourier transform of (3.14) for $\tilde{V}_{12}(r)$ would require a loop integration over the energy transfer q_0. Such an integration would greatly complicate the resulting cross-section expressions and, moreover, would require detailed information regarding the spectrum of correlations in the deuteron wave function. However, since $q_0 \ll |\boldsymbol{q}|$, it is a reasonable approximation to simply fix q_0 at some value within the kinematically allowed range, thereby avoiding the integration.

In ref. [12]), BRW adopted the value $q_0 = 0$. We prefer the choice, $q_0 = \frac{1}{2}\omega$, since it lies midway in the kinematically allowed range and maximizes the phase space available to the outgoing nucleons. Unfortunately, the cross-section results are not independent of q_0; we found that imposition of the static limit ($q_0 = 0$) yields cross sections approximately 2 mb less than ours at the peak.

The πNΔ and πNN vertex functions appearing in eq. (3.14), $f^*(q)$ and $f(q)$, respectively, are normalized to the empirical coupling constants at the pion pole. If these coupling constants are inserted in place of the vertex functions in (3.14) and the resulting expression Fourier transformed to position space, we obtain

$$V^{\pi}_{12}(\boldsymbol{r}) = \frac{1}{3}\frac{f^* f}{4\pi}\left(\frac{\mu}{m_\pi}\right)^2 \frac{\mathrm{e}^{-\mu r}}{r}\left[\boldsymbol{S}_1 \cdot \boldsymbol{\sigma}_2 + \left(1 + \frac{3}{\mu r} + \frac{3}{\mu^2 r^2}\right) S^*_{12}(\hat{\boldsymbol{r}})\right] \boldsymbol{T}_1 \cdot \boldsymbol{\tau}_2, \tag{3.15}$$

where $\mu^2 = m_\pi^2 - q_0^2$, and

$$S^*_{12}(\boldsymbol{r}) = 3\boldsymbol{S}_1 \cdot \hat{\boldsymbol{r}}\boldsymbol{\sigma}_2 \cdot \hat{\boldsymbol{r}} - \boldsymbol{S}_1 \cdot \boldsymbol{\sigma}_2 \tag{3.16}$$

is the NΔ tensor operator.

† We note that a galilean-invariant πNΔ coupling would lead to corrections in σ_{tot} of the order of 10%, according to ref. [33]).

The exchanged pion is far off-shell, however, since it carries a large momentum but little energy, and hence, it is necessary to take account of the extended structure of the vertex functions. Because the baryons are not far from their mass shell, this is most simply accomplished with the aid of form factors that are functions only of the squared 4-momentum of the pion. In the present calculations, we employ form factors of the type:

$$f(q)=f\frac{\Lambda_\pi^2-m_\pi^2}{\Lambda_\pi^2-q^2}, \qquad f^*(q)=f^*\frac{\Lambda_\pi^{*2}-m_\pi^2}{\Lambda_\pi^{*2}-q^2}, \tag{3.17}$$

that are normalized at $q^2=m_\pi^2$ to the empirical coupling constants, $f^2/4\pi=0.08$ and $f^*=2f$. The form of these factors has some theoretical basis [19,20]) and is such that the factors may easily be incorporated in eq. (3.15) with the use of a partial fraction separation during the Fourier transformation from momentum space.

Unfortunately, reliable values for the cut-offs, Λ_π and Λ_π^*, in eq. (3.17) are not available. Detailed microscopic calculations [19]) indicate that both cut-offs are of the order of 1 GeV. In addition, an upper limit for Λ_π of about 1.5 GeV is suggested by one-boson exchange models for the NN interaction [21]), but this is not necessarily definitive†. In view of these uncertainties, we have calculated cross sections for several values of the cut-offs within a range we regard as physically reasonable. In practice it is not necessary to distinguish between the two cut-offs Λ_π and Λ_π^* since they are comparable and merely multiply the internal vertices; thus we choose $\Lambda_\pi^*=\Lambda_\pi$.

3.2.2. Two-pion exchange. The other contribution to $\tilde{V}_{12}(r)$, the $2\pi(1^-)$ exchange piece, is depicted diagramatically in fig. 2.

It can be represented non-relativistically in r-space as a distributed mass exchange with the spin-isospin structure associated with an exchanged ρ-meson:

$$V_{12}^{\rho}(r)=\frac{1}{4\pi}\int_{4m_\pi^2}^{\infty}\mathrm{d}t\,t\rho^*(t)\frac{1}{3}\frac{\mathrm{e}^{-r\sqrt{t}}}{r}\left[2(\boldsymbol{S}_1\cdot\boldsymbol{\sigma}_2)-\left(1+\frac{3}{r\sqrt{t}}+\frac{3}{r^2t}\right)S_{12}^*(\hat{r})\right]\boldsymbol{T}_1\cdot\boldsymbol{\tau}_2\,. \tag{3.18}$$

Here $\rho^*(t)$ is the appropriate mass distribution function, which ideally, should be obtained from a dispersion theoretic calculation of the $\Delta\bar{\mathrm{N}}\to\pi\pi$, $J^\pi=1^-$ helicity amplitude. In the absence of such a calculation, we assume that $\rho^*(t)$ is related to $\rho(t)$, the mass distribution characterizing the $2\pi(1^-)$ exchange part of the NN interaction, by a constant scaling factor, α_ρ, equal to the ratio of the effective $\rho\mathrm{N}\Delta$ and $\rho\mathrm{NN}$ couplings; i.e.,

$$\rho^*(t)=\alpha_\rho\rho(t)\,. \tag{3.19}$$

$\rho(t)$ is, in turn, related to the square of the $\mathrm{N}\bar{\mathrm{N}}\to\pi\pi$, $J^\pi=1^-$ helicity amplitude $f_-^1(t)$ through simple kinematic and threshold factors,

$$\rho(t)=\frac{3(t-4m_\pi^2)^{3/2}}{32M^2\sqrt{t}}|f_-^1(t)|^2\,. \tag{3.20}$$

† A value $\Lambda_\pi=1.2$ GeV is obtained in a recent dispersion relation analysis [20]).

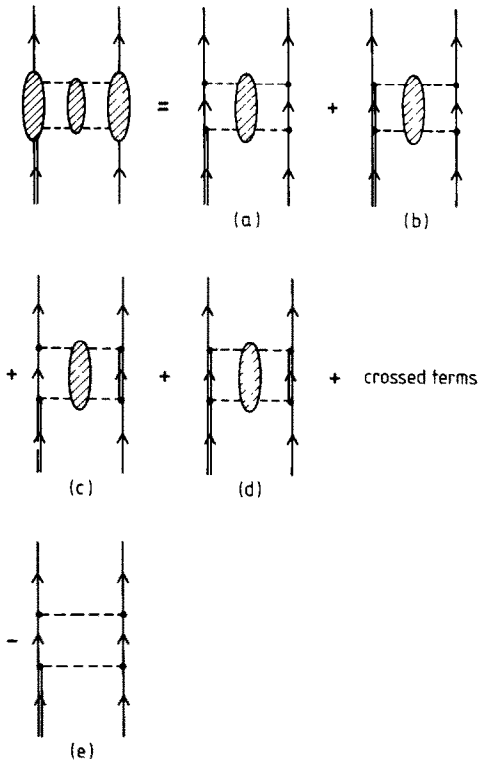

Fig. 2. Contributions to the isovector-vector two-pion exchange [$2\pi(1^-)$ exchange]. The elliptical shaded areas intersecting the pion lines indicate that the exchange may be either resonant or non-resonant. Diagram (e) is the Born term.

Eq. (3.19) is clearly an approximation, because it ignores any additional t-dependence in $\rho^*(t)$ not contained in eq. (3.20). On the other hand, if (3.19) is replaced by a δ-function distribution,

$$\rho^*(t) = \alpha_\rho \frac{f_\rho^2}{m_\rho^2} \delta(t - m_\rho^2) , \tag{3.21}$$

where m_ρ is an average "ρ-meson" mass and

$$f_\rho^2 = \int_{4m_\pi^2}^{\infty} \mathrm{d}t\, t\rho(t) , \tag{3.22}$$

with $\rho(t)$ given by eq. (3.20), the total cross section results are altered by only a few percent. This suggests that the specific form of $\rho^*(t)$ is not very important, provided its overall normalization is preserved.

The value of the scaling factor α_ρ in eq. (3.19) is a matter of some debate. The static quark model predicts either $\alpha_\rho = 1.7$ or $\alpha_\rho = 2.0$ depending upon whether the quark

model value or the Chew–Low value is adopted for the ratio f^*/f. A value in this range is further supported by considerations based on the electromagnetic NΔ transition form factor [22]), if analysed in the vector dominance model, which is expected to work better for the NΔ transition form factor than for the nucleon form factor itself. On the other hand, Kisslinger [23]) has recently proposed the value $\alpha_\rho \simeq 1.0$ on the basis of the ρ-exchange Born contribution to $\pi N \to \pi\Delta$. Since this debate has not yet been definitely resolved, we have obtained results using several different values for α_ρ.

There are also several choices available for $f^1_-(t)$, which differ primarily in the associated ρNN coupling defined by eq. (3.22). So as to be consistent with our choice for the nucleon–nucleon potential, we employ the amplitudes recently obtained by the Paris group [24]) using dispersion theoretic methods. These amplitudes correspond to an effective ρNN coupling of $f_\rho^2/4\pi \cong 4.9$ and are nearly identical to the amplitudes obtained previously by Höhler and Pietarinen [25]).

Among the contributions to $f^1_-(t)$ is the iterated OPE term depicted in diagram e of fig. 2. Since this term is already included in the OPE contribution to $\hat{M}_p$ by virtue of the final-state correlations, it must be removed from V^ρ_{12} to avoid double counting. Thus, the helicity amplitude to be inserted in eq. (3.20) is not the full amplitude, but the amplitude with the Born term subtracted. In ref. [12]) the necessary subtraction is accomplished before squaring so that the resulting amplitude, $|f^1_-(t) - f_{\rm Born}(t)|^2$, is positive definite. Such a procedure conforms with the usual definition of the ρ-meson mass distribution but, when employed in connection with (3.20), leads to the omission of certain contributions to V^ρ_{12}. This is made evident by reference to fig. 2. Clearly, the inclusion of diagrams b and c in V^ρ_{12} requires that the Born subtraction be effected after squaring. The resulting amplitude, $|f^1_-(t)|^2 - |f_{\rm Born}(t)|^2$, is no longer positive definite, but it need not be so since it now contains terms in addition to those ordinarily associated with ρ-exchange.

These additional terms are associated with 2nd-order rescattering processes of the type considered explicitly in coupled channel treatments of $\pi^+ d \to pp$. With their inclusion in V^ρ_{12} we obtain cross sections that are approximately 2.5 mb less at the peak than those obtained with the BRW prescription for $|f^1_-(t)|^2$. Although the interpretation of this result is not altogether clear, we believe that it provides a qualitative measure of the influence of multiple rescattering processes on πd disintegration.

An alternative approach would be to use the $T = 1$ $\tau_1 \cdot \tau_2$ part of the Paris NN potential and convert it directly to the N$\Delta \to$ NN transition interaction by simply employing an overall scaling factor. This would reduce the number of parameters and introduce instead an additional phenomenological short-range piece. On the other hand, much of the short-range NΔ interaction is cut out by short-range correlations in the deuteron and in the final-state pp wave function; we also prefer that the model be flexible enough that the ρNΔ coupling strength can be handled explicitly.

3.3. s-WAVE RESCATTERING

The s-wave rescattering contribution to the T-matrix, illustrated in fig. 1c, involves an effective s-wave $\pi\pi$NN vertex composed primarily of three dynamical constituents: t-channel σ- and ρ-exchange and a u-channel term comprising $\bar{\text{N}}$-exchange in combination with other short-range pieces. Fig. 3 depicts these processes diagramatically. All three processes can be conveniently represented on a phenomenological level with the aid of the zero-range lagrangian of Koltun and Reitan [13],

$$L_{\text{S}} = -4\pi\left[\frac{\lambda_1(t)}{m_\pi}\,\bar{\psi}\boldsymbol{\phi}\cdot\boldsymbol{\phi}\psi + \frac{\lambda_2(t)}{m_\pi^2}\,\bar{\psi}\boldsymbol{\tau}\cdot\boldsymbol{\phi}\times\boldsymbol{\pi}\psi\right]. \tag{3.23}$$

Here $t=(\omega-q_0)^2-(\boldsymbol{k}-\boldsymbol{q})^2$ is the 4-momentum transfer in the πN t-channel, ψ and ϕ are the nucleon and pion field operators, and π is the momentum canonically conjugate to ϕ. The first term of this lagrangian, the isoscalar piece, summarizes the σ-exchange and u-channel processes illustrated in fig. 3; the other term, of isovector nature, describes the ρ-exchange.

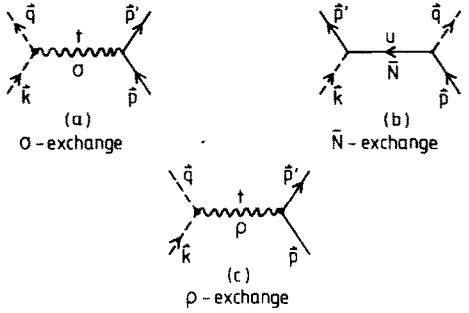

Fig. 3. Contributions to the effective $\pi\pi$NN s-wave vertex.

As discussed by Hamilton [26], the time derivative operator $\pi=\dot{\phi}$ acts symmetrically, yielding a factor $\omega+q_0$.

The phenomenological couplings, λ_1 and λ_2, in eq. (3.23) are functions of t that are related on-shell to simple linear combinations of the empirical πN s-wave scattering lengths:

$$\begin{aligned}\lambda_1(t=0) &= -\tfrac{1}{6}m_\pi(a_1+2a_3)\,,\\ \lambda_2(t=0) &= \tfrac{1}{6}m_\pi(a_1-a_3)\,.\end{aligned} \tag{3.24}$$

Using the most recently determined values for a_1 and a_3 [refs. [27,28]], these expressions yield $\lambda_1(t=0)=0.0065$ and $\lambda_2(t=0)=0.046$. The small size of the former with respect to the latter clearly indicates substantial cancellation between the σ-exchange and u-channel contributions to λ_1, at least on-shell. Because of their smooth energy dependence, the values given by eq. (3.24) will be used throughout the energy range of interest to us.

If we neglect the t-dependence of λ_1 and λ_2 by inserting their on-shell values into eq. (3.23), we obtain

$$\hat{M}_s(\boldsymbol{k}, \boldsymbol{r}) = -i\frac{f}{m_\pi}\left(\frac{\mu}{m_\pi}\right)\left(1+\frac{1}{\mu r}\right)\frac{e^{-\mu r}}{r}$$
$$\times\left\{e^{i\boldsymbol{k}\cdot\boldsymbol{r}/2}(\boldsymbol{\sigma}_2\cdot\hat{\boldsymbol{r}})\sqrt{2}\left[2\lambda_1\tau_{2+}-i\frac{\lambda_2}{m_\pi}(\omega+q_0)(\boldsymbol{\tau}_1\times\boldsymbol{\tau}_2)_+\right]\right.$$
$$\left.-e^{-i\boldsymbol{k}\cdot\boldsymbol{r}/2}(\boldsymbol{\sigma}_1\cdot\hat{\boldsymbol{r}})\sqrt{2}\left[2\lambda_1\tau_{1+}+i\frac{\lambda_2}{m_\pi}(\omega+q_0)(\boldsymbol{\tau}_1\times\boldsymbol{\tau}_2)_+\right]\right\} \quad (3.25)$$

for the s-wave rescattering contribution to the T-matrix in r-space. However, because the pion exchanged between the two nucleons in the rescattering process is far off-shell and hence, t is significantly less than zero, we cannot neglect the t-dependence of the couplings. To describe this t-dependence, it is necessary to reconsider the dynamical contributions to L_s in somewhat more detail. The contribution from ρ-exchange has a particularly simple dependence on t, just $(m_\rho^2-t)^{-1}$, where m_ρ is the ρ-meson mass. This suggests an off-shell extrapolation of λ_2 of the form

$$\lambda_2(t) = \lambda_2\frac{m_\rho^2}{m_\rho^2-t} \cong \lambda_2\frac{m_\rho^2}{m_\rho^2+\frac{3}{4}\omega^2-m_\pi^2+\boldsymbol{q}^2}, \quad (3.26)$$

where λ_2 on the r.h.s. is given by eq. (3.24) and in the second, approximate equality the average value $q_0=\frac{1}{2}\omega$ has been used and the angle-dependent term in $(\boldsymbol{k}-\boldsymbol{q})^2$ dropped.

The isoscalar coupling is more difficult to treat due to the more complicated structure of its dynamical contributions. In analogy with ρ-exchange, the t-dependence of the σ-exchange amplitude is just $(m_\sigma^2-t)^{-1}$; however, the u-channel amplitude cannot be described unambiguously in so simple a fashion. Rather than embark on a complicated analysis of this amplitude, we assume that it has a sufficiently short effective range that it does not influence the off-shell behaviour of λ_1 in the momentum range considered. Considering the fact that a large part of this contribution involves $N\bar{N}$ intermediate states, such an assumption is not altogether unjustified.

With this assumption, the off-shell structure of λ_1 can be cast in the form

$$\lambda_1(t) = -\tfrac{1}{2}m_\pi\left[a_{sr}+a_\sigma\frac{m_\sigma^2}{m_\sigma^2-t}\right]$$
$$\cong -\tfrac{1}{2}m_\pi\left[a_{sr}+a_\sigma\frac{m_\sigma^2}{m_\sigma^2+\frac{3}{4}\omega^2-m_\pi^2+\boldsymbol{q}^2}\right], \quad (3.27)$$

where $3a_{sr}$ and $3a_\sigma$ are the short-range and σ-exchange contributions to the on-shell amplitude a_1+2a_3. We choose $m_\sigma \cong 4.2\, m_\pi$ for the σ-meson mass. In the second

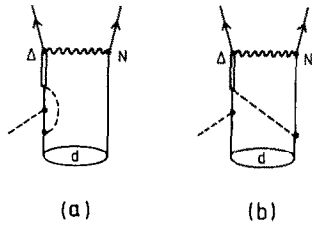

Fig. 4. (a) Crossed nucleon Born contribution to the external $\pi N\Delta$ vertex. (b) A diagram of the same order that partly cancels (a) (note the time-ordering of the πNN vertices).

equality the same approximations have been employed as in eq. (3.26). Following Hamilton [26]), we adopt the value $a_\sigma = 0.22\ m_\pi^{-1}$ so that

$$a_{sr} = \tfrac{1}{3}(a_1 + 2a_3 - 3a_\sigma) = -0.23 m_\pi^{-1}\,. \tag{3.28}$$

The vertex functions $\lambda_1(t)$ and $\lambda_2(t)$, given by eqs. (3.26) and (3.27), respectively, specify the off-shell extrapolation of the $\pi\pi NN$ vertex involved in the s-wave rescattering process. To describe the off-shell structure of the p-wave πNN vertex in this process, we employ a form factor of the type given by eq. (3.17). All three functions are easily incorporated in eq. (3.25) for the s-wave rescattering contribution to the T-matrix my means of partial fraction separations.

Because of the t-dependence in eq. (3.27), the approximate cancellation on-shell between the σ-exchange and u-channel contributions to λ_1 is destroyed off-shell with the result that λ_1 and λ_2 can be of the same order of magnitude. Although this might be expected to significantly alter the T-matrix contributions given by eq. (3.25), it has little effect on the cross sections except near threshold, where the s-wave rescattering mechanism dominates in the absence of recoil terms.

3.4. MATRIX ELEMENTS

To obtain the matrix elements of the various T-matrix contributions discussed above, we have adopted a formalism rather different from that of ref. [12]), where matrix elements must be evaluated separately in each partial wave of the relative pp state. In the present formalism the initial and final nucleon states, together with the incoming pion wave function, are decomposed into partial waves and recoupled in such a way that the relevant matrix elements can be easily evaluated in arbitrary angular momentum channels. Details of this procedure together with explicit expressions for the matrix elements may be found in appendix B.

4. Results

In this section we report the results of total and differential cross section calculations for $\pi^+ d \rightleftarrows pp$ using the model described in the previous section. Most of the

results were obtained with the Paris NN interaction; however, we have also included some results obtained with the Reid potential for comparison purposes. The deuteron wave functions derived from the Paris interaction were kindly supplied to us by the Paris group, while those derived from the Reid potential were taken from ref. [29]). To obtain the relative pp wave functions, we solved the Schrödinger equation with correlations in each partial wave with angular momentum $l_{pp} \leq 2$, neglecting the weak tensor coupling of the $^3P_2$ and $^3F_2$ states. For $l_{pp} > 2$, the appropriate spherical Bessel functions were employed. If correlations are extended to the f-waves, the calculated cross sections are altered by less than 1% over the whole range of momenta considered.

For calculation of the total cross section, the partial wave expansion of the relative pp state may be safely truncated at $l_{pp} = 4$; inclusion of higher partial waves perturbs the total cross section result almost imperceptibly. In differential cross section calculations, however, higher partial waves exert a significant influence. In this connection we note that the particular parametrization of $d\sigma/d\Omega$ by means of a power series in $\cos^2\theta$ has major disadvantages. A more natural representation would be in terms of a Legendre expansion,

$$\frac{d\sigma}{d\Omega} = \sum_{i=0}^{\infty} u_{2i} P_{2i}(\cos\theta). \tag{4.1}$$

The u's converge quite well as the number of partial waves included in the relative pp state is increased. This is not true for the γ's: if expressed in the form $\gamma_i = \sum_{j>i} A_{ij} u_j$, the expansion coefficients A_{ij} increase rapidly with both i and j. Thus, for example, the coefficient γ_4 receives significant contributions from higher partial waves via the u_6 and u_8 coefficients. Although eq. (4.1) is clearly a superior parametrization to eq. (1.1), nearly all the empirical results are parametrized according to eq. (1.1); hence, we employ the power series form in the present calculations. It is then necessary to include partial waves up to $l_{pp} = 6$ to ensure convergence in γ_4.

4.1. THE TOTAL ABSORPTION CROSS SECTION

In fig. 5 the total absorption cross section obtained with the Paris potential is illustrated as a function of the c.m. momentum for various values of the parameters α_ρ and Λ_π. The solid curves here correspond to the choice $\alpha_\rho = 1.7$, the dashed curves to $\alpha_\rho = 2.0$. In none of the results illustrated were recoil corrections included. Note that an increase in the cross section induced by a decrease in the $\rho N\Delta$ coupling α_ρ can be offset by a decrease in the form factor cut-off Λ_π. This indicates, as observed already in ref. [12]), that the dynamics responsible for the total cross section are largely governed by the tensor interaction, so that the effect of $2\pi(1^-)$ exchange can be simulated by a renormalization of the πNN form factor. This is not true for the differential cross section, however, as will be made evident in the next subsection.

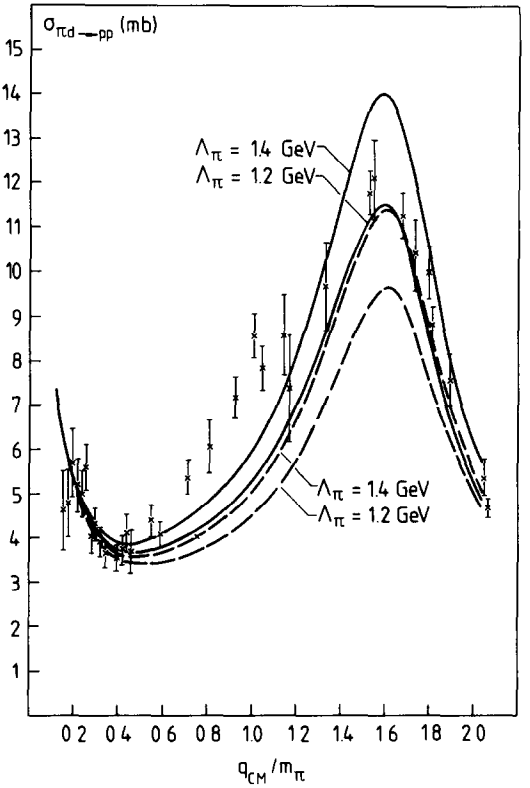

Fig. 5. $\sigma_{\pi d \to pp}$ without recoil corrections versus $q_{c.m.} = k_{\pi d}$ for the Paris potential and various values of the parameters α_ρ and Λ_π. The solid curves were obtained with $\alpha_\rho = 1.7$, the dashed curves with $\alpha_\rho = 2.0$. The empirical values are from refs. [4,6]).

Fig. 6 illustrates the interaction dependence of the cross section for two values of Λ_π. In this figure results obtained with the Paris potential are indicated by solid lines, Reid potential results with dashed lines. Again, recoil corrections have not been included. As a function of the c.m. momentum, the qualitative behaviour of the cross sections derived from the two potentials is similar, though the Reid results lie somewhat above the Paris results for a particular choice of parameters. With either potential the empirical results can be fit reasonably well near the peak; using the Paris potential and $\alpha_\rho = 1.7$, a value $\Lambda_\pi = 1.2$ GeV is required. A somewhat lower value is required if the Reid potential is employed.

The influence of recoil corrections of the type discussed above in connection with eq. (3.2) is exhibited in fig. 7. All three curves in this figure were obtained with the Paris potential and the parameters $\alpha_\rho = 1.7$ and $\Lambda_\pi = 1.2$ GeV. Comparing the two curves labelled "no recoil" and "PS recoil", we see that the inclusion of pseudoscalar recoil corrections in the expression for $\hat{M}_{IA}$ has little effect on the total cross section except at low energy. This result is peculiar to the total cross section and arises from a

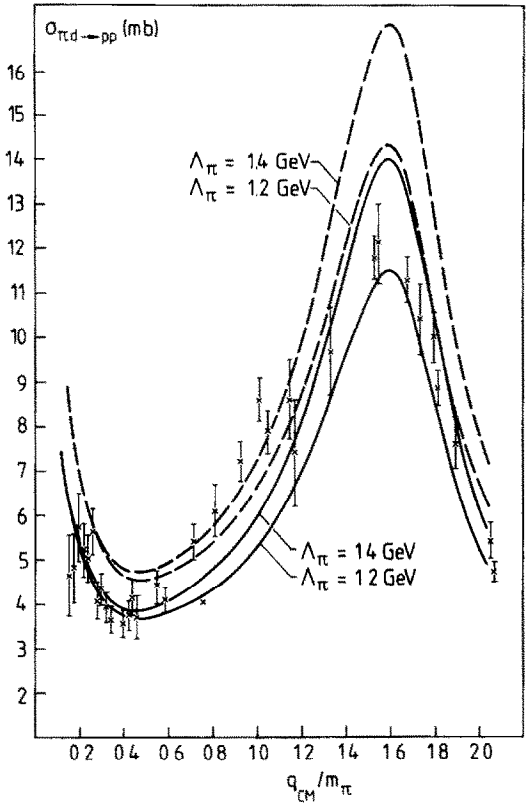

Fig. 6. $\sigma_{\pi d \to pp}$ without recoil corrections for the Paris potential (solid curves) and Reid potential (dashed curves) using $\alpha_\rho = 1.7$ and two values for Λ_π.

fortuitous balancing of effects among different partial wave contributions to the cross section. On the other hand, the influence of pseudovector recoil terms is quite pronounced even at high energy. Of course, we should not overlook the approximations upon which our treatment of the recoil terms has been based (e.g., the use of plane wave Dirac spinors in the non-relativistic reduction). Our results indicate the magnitude of recoil effects, but should not be regarded as definitive.

We have studied the relative importance of the different mechanisms incorporated in our model for pion absorption by computing the cross sections arising from different contributions to the T-matrix. The results are shown in fig. 8 for the case of no recoil corrections (solid lines) and pseudovector recoil corrections (dashed lines). In both cases, it is clear that the resonance structure of the cross sections arises from the p-wave rescattering mechanism and that this mechanism provides the largest contribution to the cross section near the peak. p-wave rescattering cannot wholly account for the magnitude of the peak, however; if the IA contribution is not included, we get only two thirds of the required magnitude, despite the fact that the

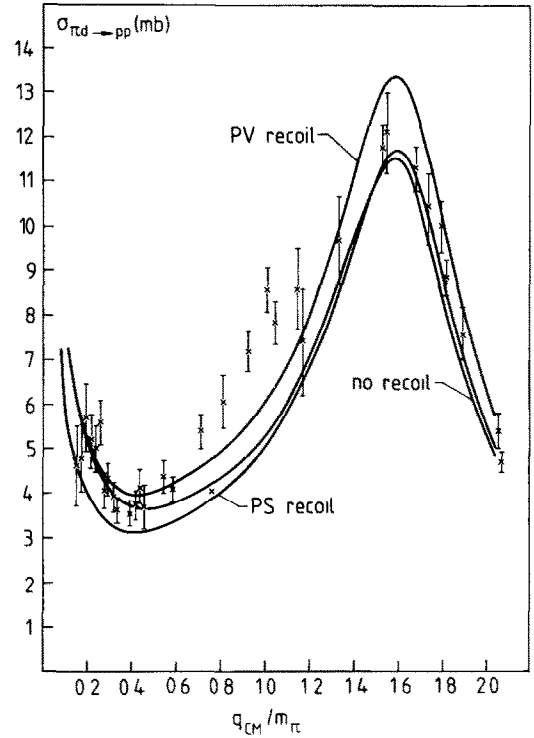

Fig. 7. $\sigma_{\pi d \to pp}$ versus $q_{c.m.} = k_{\pi d}$ for the Paris potential and the parameters $\alpha_\rho = 1.7$ and $\Lambda_\pi = 1.2$ GeV using various models for the recoil corrections. The curve labelled "no recoil" was obtained with $\alpha = \beta = 0$ in eq. (3.7), while the curves labelled "PS recoil" and "PV recoil" were obtained respectively with the pseudoscalar and pseudovector choices for these parameters.

IA contribution alone yields a relatively small, non-resonant cross section in the peak region. This underscores the importance of interference terms in the total cross section.

As expected, the influence of recoil terms on the cross section is evinced most dramatically in the results obtained with the impulse approximation alone. Without recoil corrections, the IA cross section is flat everywhere, increasing strongly with momentum near threshold but never exceeding 2 mb. When pseudovector recoil terms are added, not only is the cross section increased in magnitude, but its momentum dependence is reversed, so that instead of increasing with momentum, it decreases. Near threshold, inclusion of recoil corrections makes the IA term the most important contribution to the T-matrix.

In the absence of recoil terms, the threshold behaviour of the cross section is governed primarily by s-wave rescattering, as a comparison of the upper two solid curves in fig. 8 reveals. This process also influences the cross section in the peak region through interference with the p-wave rescattering process. Note that the

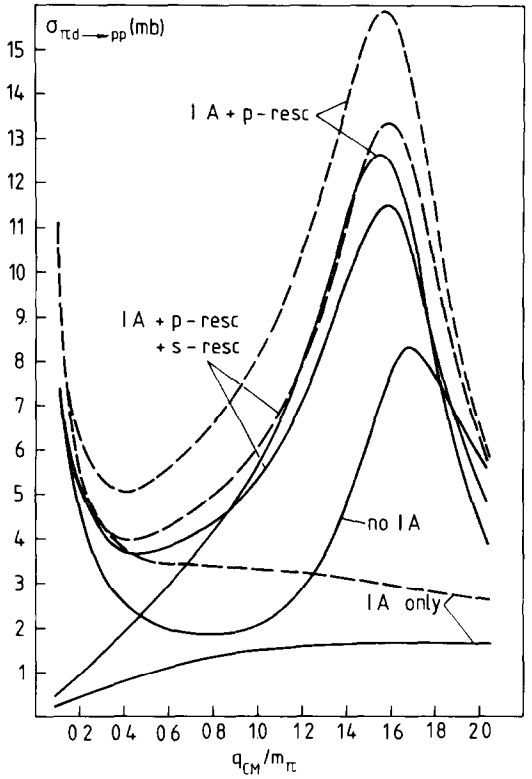

Fig. 8. Paris potential cross sections for $\alpha_\rho = 1.7$ and $\Lambda_\pi = 1.2$ GeV arising from different contributions to the T-matrix as depicted in fig. 1. The solid curves were obtained with no recoil corrections, the dashed curves with pseudovector recoil corrections.

interferences between the s- and p-wave rescattering terms and the s-wave rescattering and IA terms are both destructive.

Fig. 9 illustrates the contributions to the total cross section from different partial waves in the relative pp state. As in fig. 8, the solid curves were obtained without recoil corrections, the dashed curves with pseudovector recoil corrections. In both cases, the dominant contribution near threshold comes from the p-wave, which in this momentum region, arises primarily from the action of s-wave rescattering and recoil terms on the deuteron s-wave and the s-wave of the pion. The p-wave also makes a significant contribution in the peak region, but in the absence of recoil terms is dominated there by the d-wave contribution, which is associated primarily with the tensor interaction operating on the deuteron and pion s-waves.

The major significance of the d-wave contribution, however, is not its magnitude, but the fact that it accounts for nearly all the difference in the Paris and Reid cross sections exhibited in fig. 6. We can understand this result in terms of the tensor interaction associated with the d-wave. The tensor interaction acts differently on the

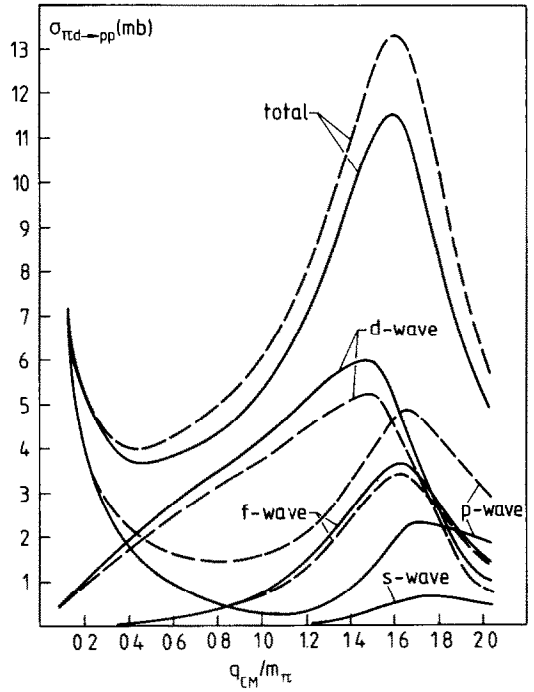

Fig. 9. Contributions to $\sigma_{\pi d \to pp}$ from different partial waves in the relative pp state for the Paris potential and the parameters $\alpha_\rho = 1.7$, $\Lambda_\pi = 1.2$ GeV. The solid curves were obtained with no recoil corrections, the dashed curves with pseudovector recoil corrections.

Paris and Reid deuteron wave functions, in part because of the different d-state probabilities characterizing the two wave functions (note that the pp d-wave is connected with the deuteron d-state, as well as the s-state, via the tensor force), but more importantly perhaps, because of the different short-range properties of the two wave functions. The tensor interaction is peaked around 1 fm. Thus, its contribution to the T-matrix is sensitive to the short-range part of the deuteron wave functions through the overall normalization, which, except for the d-state probability, is interaction independent. Compared with the Reid deuteron, the Paris deuteron has more of its wave function concentrated at short range and therefore, less around 1 fm. Consequently, the tensor interaction makes a smaller contribution to the T-matrix with the Paris deuteron, and the Paris cross section is smaller.

Of the remaining partial wave contributions, only that from the pp f-wave is significant. This contribution arises from the action of the tensor on the deuteron s-wave and pion p-wave and is seen in fig. 9 to be quite sizeable in the peak region. The s-wave makes only a small contribution to the cross section near resonance, while that of the g-wave and higher partial waves is almost negligible.

Comparison of the dotted and solid curves in fig. 9 reveals that recoil terms exert their strongest influence on the pp p-wave contribution, which is significantly

increased by their inclusion. The d-wave contribution is also affected, decreasing somewhat as recoil terms are added. For the pseudovector case shown in the figure, the increase in the p-wave contribution greatly outweighs the decrease in the d-wave contribution, so that recoil terms increase the total cross section overall. For the pseudoscalar case, on the other hand, the p-wave increase is more moderate and is largely offset by the decrease in the d-wave contribution. Thus, including recoil terms of pseudoscalar type has little overall effect on the cross section.

4.2. THE DIFFERENTIAL CROSS SECTION

The power series coefficient γ_0 in eq. (1.1) for the pion production differential cross section is shown in fig. 10 for the Paris and Reid potentials (indicated with solid

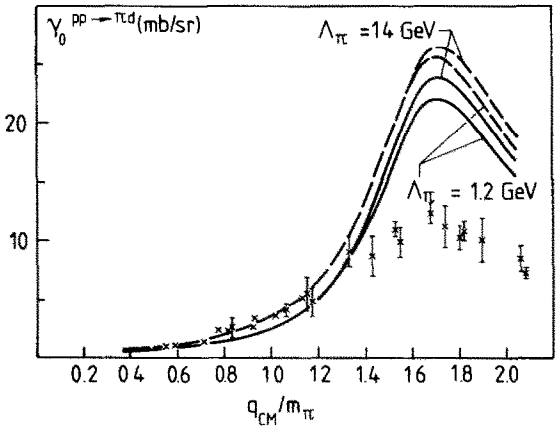

Fig. 10. γ_0 without recoil corrections versus $q_{c.m.} = k_{\pi d}$ for the Paris and Reid potentials using $\alpha_\rho = 1.7$ and two values of Λ_π. Notation as in fig. 6. the empirical values are from ref. [8]).

and dashed lines respectively) and for two choices of the parameter Λ_π. The results exhibited were all obtained with $\alpha_\rho = 1.7$, but the results with $\alpha_\rho = 2.0$ are very similar. None of the curves include recoil corrections. As can be seen, γ_0 can be increased somewhat by substituting the Reid potential for the Paris potential or by increasing Λ_π. By and large, though, γ_0 is not very sensitive either to the parameters or the interaction, which is disconcerting in view of the large discrepancy between the calculated and empirical results. A possible explanation for this discrepancy may lie in elastic distortion effects not included in the present model. Such effects, induced by elastic πd scattering prior to the absorption process, tend to increase the effective Δ_{33} width that regulates the p-wave rescattering process and thus lower γ_0. We will consider this point further in the next section.

Results for the coefficient γ_2 without recoil corrections are illustrated in fig. 11 for the Paris potential and various parameter choices. In this figure the solid curves

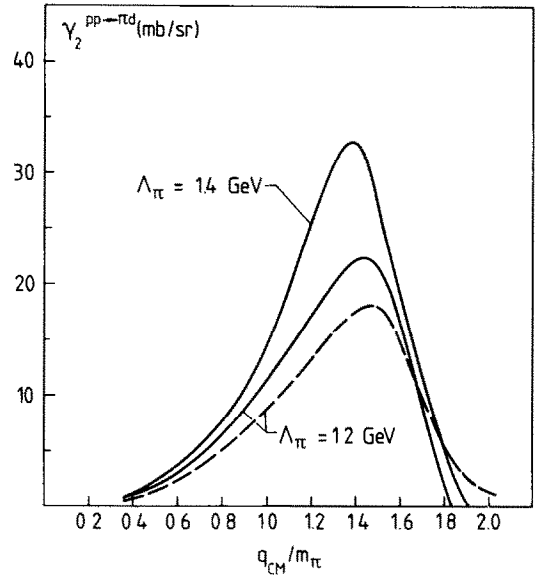

Fig. 11. γ_2 without recoil corrections versus $q_{c.m.} = k_{\pi d}$ for the Paris potential and various values of α_ρ and Λ_π. Notation as in fig. 5. The empirical values are from ref. [8]).

correspond to $\alpha_\rho = 1.7$, the dashed curves to $\alpha_\rho = 2.0$. By and large, the parameter dependence of γ_2 is similar to that of the total cross section, although the dependence on α_ρ here is somewhat weaker.

The interaction dependence of γ_2 is illustrated in fig. 12 where the solid curves indicate Paris potential results and the dashed curves Reid potential results, again without recoil corrections. This figure looks much like fig. 6, revealing that γ_2 and the total cross section have similar interaction dependences. In comparison with the empirical results, however, the calculated γ_2 lies too low at high energies for a parameter choice that yields a good fit to the total cross section. This is partly a consequence of the poor γ_0 results, due to the approximate proportionality between $\sigma_{\pi d\to pp}$ and the combination $\gamma_0 + \frac{1}{3}\gamma_2$ (neglecting higher-order terms in the power series). Clearly, if we choose parameters to fit γ_2, the theoretical overestimate of γ_0 would necessarily result in an overestimate of the total cross section. In addition to this insufficient magnitude, the γ_2 results also seem to be shifted slightly to the left relative to the empirical results.

The coefficients γ_0 and γ_2 both behave much like the total cross section as functions of the interaction and the parameters and thus, do not provide much new information. Far more interesting is the coefficient γ_4. In contrast to γ_0 and γ_2, γ_4 turns out to be only weakly dependent on Λ_π and the interaction (Paris versus Reid). It depends quite strongly on the parameter α_ρ, however. This can be seen in fig. 13, where we exhibit the γ_4 obtained without recoil corrections using the Paris potential for $\Lambda_\pi = 1.2$ GeV and several values of α_ρ. The strong α_ρ dependence manifested

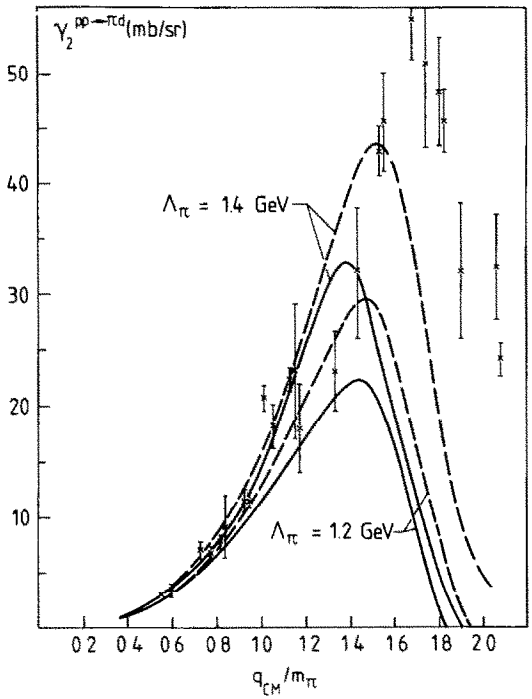

Fig. 12. γ_2 without recoil corrections for the Paris and Reid potentials using $\alpha_\rho = 1.7$ and two values of Λ_π. Notation as in fig. 6.

here, in combination with the weak Λ_π and interaction dependences, makes γ_4 a discriminant among different models for the $\rho N\Delta$ vertex. At present, the empirical data do not permit a very fine discrimination, but they do limit the acceptable range of values for α_ρ. We note, in particular, that Kisslinger's [23]) value for α_ρ yields a γ_4 that is large and positive in the resonance region. This is clearly inconsistent with the data. On the other hand, an α_ρ value near 2.0 yields a γ_4 well within the acceptable range.

The effect of recoil corrections on the γ coefficients is illustrated in figs. 14–16. Such corrections have only a moderate effect on γ_0, increasing it slightly, but have a rather large effect on γ_2. For the pseudovector case, γ_2 is doubled in the resonance region when recoil terms are added. This increase is large enough that with recoil terms included the right order of magnitude can be attained for both γ_2 and the total cross section with the same set of parameters, although the peak in the γ_2 results is still somewhat too low and shifted to the left relative to the empirical results. Unfortunately, as revealed in fig. 16, recoil terms also significantly influence γ_4, decreasing it substantially at low and intermediate energies. Clearly, any gain in the quality of the γ_2 fit obtained by including recoil corrections must be paid for with a decline in the quality of the γ_4 fit.

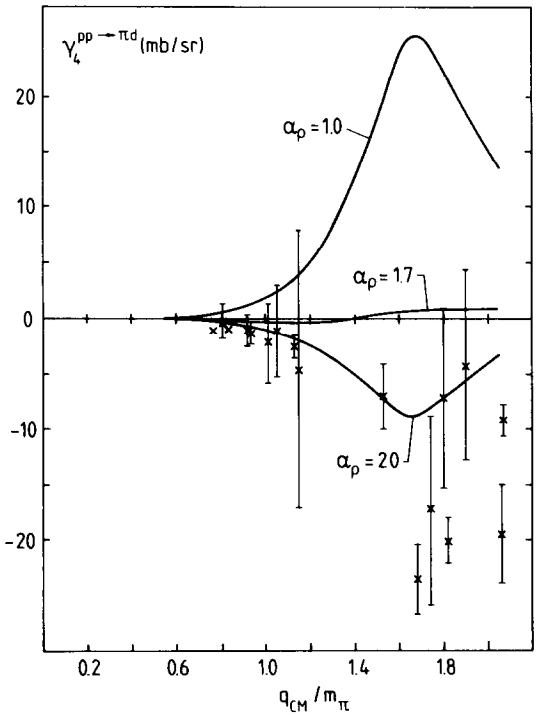

Fig. 13. γ_4 without recoil corrections for the Paris potential and $\Lambda_\pi = 1.2$ GeV using various values of α_ρ. The empirical values are from ref. [8]).

Aside from the convergence difficulties discussed at the beginning of this section, the $\cos^2\theta$ power series expansion itself converges rather poorly. We found in particular, that although $\gamma_4 \geqslant \gamma_6$ for large (in magnitude) values of γ_4, for quite small values of γ_4, γ_6 may be as much as an order of magnitude larger than γ_4. In such a

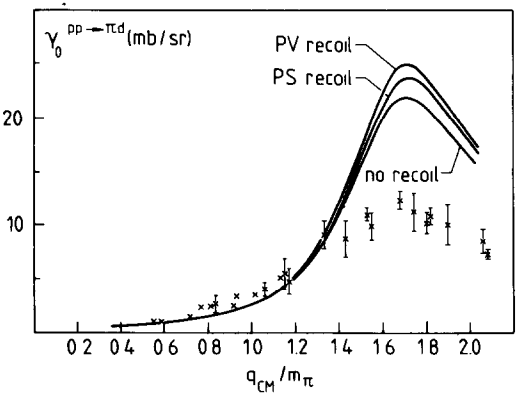

Fig. 14. γ_0 versus $q_{c.m.}/m_\pi$ for the Paris potential and various models for the recoil corrections. Parameters and notation as in fig. 7.

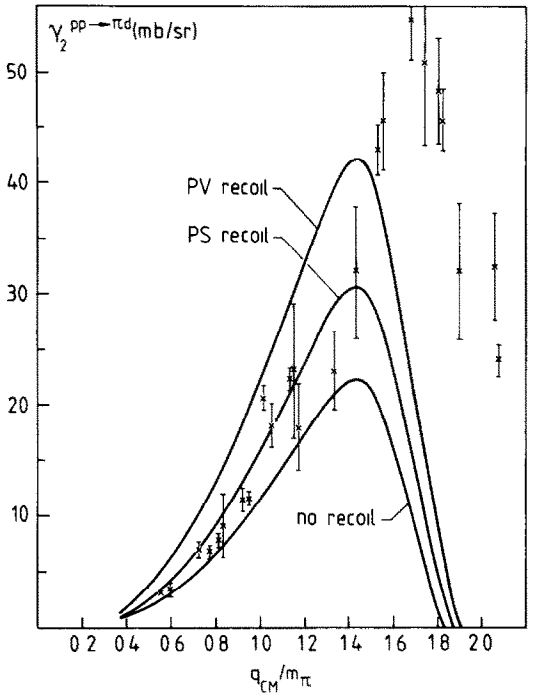

Fig. 15. γ_2 versus $q_{\text{c.m.}}/m_\pi$ for the Paris potential and various models for the recoil corrections. Parameters and notation as in fig. 7.

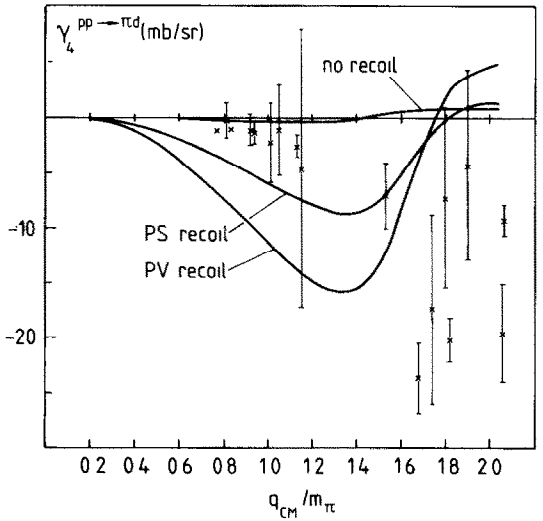

Fig. 16. γ_4 versus $q_{\text{c.m.}}/m_\pi$ for the Paris potential and various models for the recoil corrections. Parameters and notation as in fig. 7.

case, we would expect the calculated γ_4 to be rather different from that obtained through a parametrization of empirical data neglecting sixth and higher order terms. This poor convergence is a peculiarity of the power series expansion, eq. (1.1); such difficulties do not affect the Legendre expansion, eq. (4.1).

In view of these convergence problems, it is useful to treat the angular distributions directly. Representative results with $\alpha_\rho = 1.7$ are illustrated in figs. 17 and 18 for two values of T_π, the laboratory kinetic energy in the pion absorption process, and for the Paris and Reid potentials respectively. Recoil corrections have not been included in these results except for the two dashed curves in fig. 17, which include pseudovector recoil terms.

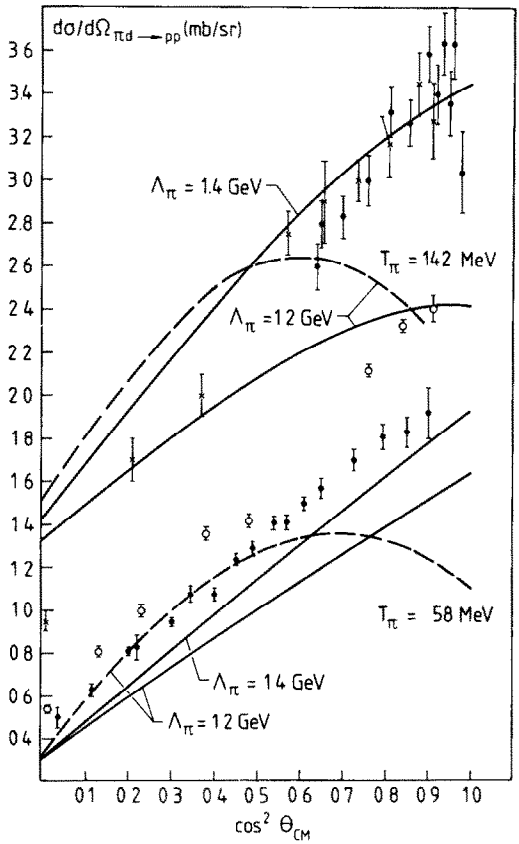

Fig. 17. Angular distributions obtained with the Paris potential using $\alpha_\rho = 1.7$ and $\Lambda_\pi = 1.2$ GeV and 1.4 GeV for $T_\pi = 58$ MeV (lower curves) and $T_\pi = 142$ MeV (upper curves). The solid curves were obtained with no recoil corrections, the dashed curves with pseudovector recoil corrections. The empirical points denoted with solid circles are from ref. [5]) and correspond to $T_\pi = 56$ and 143 MeV; the open circles, corresponding to $T_\pi = 60$ MeV, and the ×'s, corresponding to $T_\pi = 142$ MeV, are from refs. [6,4]) respectively.

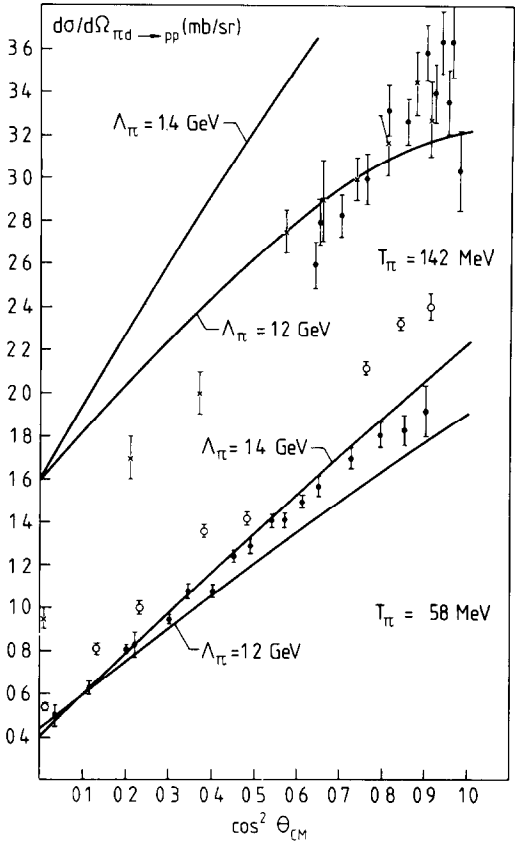

Fig. 18. Angular distributions obtained with the Reid potential. Parameters and notation as in fig. 17.

Despite the general lack of agreement between the calculated and empirical γ-coefficients, the calculated angular distributions are not bad, at least when recoil terms are omitted. At $T_\pi = 58$ MeV, corresponding to $q_{\text{c.m.}} = 0.9 m_\pi$, the Reid results with $\Lambda_\pi = 1.4$ GeV nearly coincide with the data. The Paris potential with the same Λ_π also yields approximately the right slope but underestimates the total cross section, so that the resulting distribution lies too low.

At $T_\pi = 142$ MeV, near the resonance peak in the total cross section, the calculated angular distributions are clearly influenced by higher terms in the power series parametrization of $\mathrm{d}\sigma/\mathrm{d}\Omega$ than are included in the empirical parametrization. At this energy, the γ_2 calculated with the Paris potential and the parameters $\alpha_\rho = 1.7$ and $\Lambda_\pi = 1.4$ GeV is only about half the empirical γ_2 (see fig. 11). Nevertheless, the average slope of the corresponding angular distribution is nearly correct. Moreover, the curvature of the distribution is negative, even though the calculated γ_4 is small and positive. The origin of this apparent discrepancy lies in the next coefficient γ_6 which is negative and an order of magnitude larger than γ_4 for this case. Evidently,

the γ_4 obtained through a least-squares fit of the empirical distribution mocks up the effect of several terms in the power series for the calculated distribution and may be completely unrelated to the calculated γ_4.

When pseudovector recoil terms are included, the calculated γ_4 and γ_6 for $\alpha_\rho = 1.7$ are both negative and of the same order of magnitude. This leads to a large negative curvature in the resulting distributions, as seen in the dashed curves in fig. 17, that cannot be reconciled with the data.

5. Discussion and conclusions

The model outlined in sect. 3 incorporates the minimum number of basic πd mechanisms necessary in order to successfully describe the main features of the total and (with somewhat less accuracy) differential π^+d$\leftrightarrow$pp cross sections. However, to obtain detailed quantitative agreement with experiment, further corrections have to be included. Estimates of effects not treated explicitly in the model will be presented in the following.

Multiple scattering of the pion in the elastic πd channel before absorption leads to a distortion of the pion wave. In the region of the 3,3 resonance, assuming Δ-dominance, a simple estimate of this effect can be obtained by observing that the difference between single and multiple πd scattering (at least at forward angles) can be translated into an effective increase of the Δ-width of about 20%, with no shift of the Δ mass, in accordance with the measured total πd cross section [31]). Inclusion of such elastic broadening in our πd$\leftrightarrow$pp calculation lowers the total cross section by about 15% in the peak region. Also, the angular distribution coefficient γ_0 is reduced by roughly the same amount at $q_{\text{c.m.}} = 1.6 m_\pi$, without affecting the low-momentum behaviour.

A further increase of the Δ-width below resonance is provided by the crossed Born terms in the $\Delta \to \pi$N decay. While it has been argued in subsect. 3.2 that the leading u-channel corrections to the πNΔ vertex, fig. 4a, are partly cancelled by related two-body diagrams, fig. 4b, such cancellations do not occur to a significant degree in the case of the Δ width Γ, because of isospin selection rules. It is therefore legitimate to multiply Γ by the corresponding u-channel form factor, which according to ref. [32]) can be converted into the approximate form $(M_\Delta^2 - M^2)/(s - M^2)$, where $\sqrt{s}$ is the πN c.m. energy. Note that this factor reduces in the static limit to ω_R/ω, the form familiar from Chew-Low theory, where $\omega_R = M_\Delta - M$. Inclusion of this effect lowers $\sigma(\pi\text{d} \to \text{pp})$ by about 10% in the peak region.

The combined effect of distortions and u-channel corrections to the width reduces γ_0 by about 25% in the region $q_{\text{c.m.}} = 1.5 - 1.8 m_\pi$. While significant, this reduction is still not quite sufficient to completely remove the discrepancies shown in fig. 10 or fig. 14. Replacement of the standard choice, eq. (3.12), for the πNΔ coupling strength by the strong coupling value $f^{*2}/4\pi = 0.37$ $(M/\sqrt{s})$ raises $\sigma(\pi\text{d} \to \text{pp})$ by about 2 mb at the peak.

At low energies s-wave rescattering and recoil corrections to the impulse approximation dominate. Our off-shell extrapolation of the s-wave rescattering amplitude should be compared with other models, like that of ref. [20]), where t-channel exchange of a ρ-meson does not appear explicitly. However, above $q_{\mathrm{c.m.}} = 0.5 m_\pi$ we find no great dependence of the results on the particular form of the off-shell extrapolation, so that no attempts have been made to further refine the off-shell model. The recoil problem cannot be resolved satisfactorily in the present model; it ultimately requires calculations with a relativistic deuteron wave function.

Our description of the $2\pi(1^-)$ exchange $\Delta N \to NN$ interaction is made conceptually consistent with the basic philosophy of the Paris potential by using the corresponding helicity amplitudes f^1_-. One of the important parameters is then α_ρ, the ratio of the $\rho N\Delta$ to ρNN coupling strength. We have pointed out that our treatment of the squared helicity amplitude in the form $|f^1_-|^2 - |f_{\mathrm{Born}}|^2$ incorporates already second-order rescattering processes which would otherwise appear in the coupled channels approach of Niskanen [11]), and which account for a 20% reduction of $\sigma(\pi d \to pp)$ in the peak region. This example also demonstrates that the proper treatment of ρ-exchange cannot be made independent of the details of the particular coupled-channels scheme employed, if 2π exchange degrees of freedom are treated explicitly.

This leads to the question about the importance of higher-order coupled-channel contributions. From a comparison with ref. [11]), which can be made using the Reid potential, cutoffs $\Lambda_\pi = 1.4$ GeV, and a strong $\rho N\Delta$ coupling, it appears that a large part of the coupled channel effects is already accounted for once second-order rescattering processes are included by a proper treatment of the squared helicity amplitude. The additional influence of the diagonal $N\Delta \to N\Delta$ interaction [V_3 of ref. [11]), not considered in our model] is to reduce $\sigma(\pi d \to pp)$ by about 10% in the peak region. The γ_0 and γ_2 coefficients obtained by Niskanen show similar discrepancies with experiment as ours, although these discrepancies are somewhat hidden in ref. [11]) by treating ratios of the γ's. We find that, at the level of total and unpolarized differential cross sections, and in situations where a meaningful comparison can be made, higher-order coupled channel contributions (in addition to the second-order processes already taken into account) are not of great importance.

Concerning the expansion in pp partial waves, we have gone considerably beyond earlier work and found that, at least for the coefficient γ_4 in $d\sigma/d\Omega$, it is absolutely necessary to incorporate angular momenta as high as $l_{pp} = 6$ to obtain convergence in the 3, 3 resonance region.

Questions of comparison with the coupled-channels approach and about the influence of partial wave truncation will be raised again in connection with polarized cross sections, to be discussed in the following paper [35]).

We mention that in the absence of recoil corrections, and if the subtraction of Born terms in the 2π exchange $N\Delta \to NN$ interaction is made according to $|f^1_- - f_{\mathrm{Born}}|^2$, our results for $\sigma(\pi d \to pp)$ and for the γ-coefficients are consistent with those of Chai and

Riska [14]), provided that a comparable set of cutoff parameters and $\rho N\Delta$ couplings is used. Again, more detailed comparisons will be made for the parameters related to polarized cross sections [35]).

One of the significant results of this work is that γ_4 depends sensitively on the $\rho N\Delta$ coupling parameter α_ρ, while its dependence on the πNN and $\pi N\Delta$ vertex cutoffs Λ_π and Λ_π^*, as well as its sensitivity to the interaction used (Reid versus Paris), is quite weak. This feature is related to the particular combinations of short-range mechanisms in higher partial waves which contribute to γ_4. Thus, if higher-quality data for γ_4 were available, constraints could be imposed selectively on α_ρ; on the other hand, $\sigma_{\rm tot}$ and γ_2 depend on both α_ρ and cutoffs in such a way that increasing α_ρ can be compensated by increasing Λ_π. We have found that small values of α_ρ, as suggested by some authors, lead to large positive values of γ_4 in the resonance region which seem to be inconsistent with presently existing (though poor quality) data. We therefore suggest that models with weak or zero isovector two-pion coupling to the $N\Delta$ system [10,16,23]) be confronted with such more detailed investigations.

Our conclusion is that values of the πNN and $\pi N\Delta$ cutoffs, $\Lambda_\pi = 1.2$–1.4 GeV, together with a relatively strong $\rho N\Delta$ coupling, $\alpha_\rho = 1.7$–2.0, are consistent with the main features of the $pp \leftrightarrow d\pi^+$ differential and total cross sections, although difficulties in understanding quantitative details of $d\sigma/d\Omega$ still remain to be resolved.

We are grateful to R. Vinh Mau for useful comments and for providing us with the latest version of the Paris potential. We also acknowledge helpful discussions with F. Myhrer, D.O. Riska and K. Shimizu.

Appendix A

KINEMATICAL RELATIONS

Consider a pion with laboratory momentum $\boldsymbol{k}$ and lab energy $\omega = \sqrt{k^2 + m_\pi^2}$ incident on an A-nucleon system of total mass $M_{\rm A}$. The invariant mass squared, evaluated in the lab system, is

$$s = m_\pi^2 + M_{\rm A}^2 + 2\omega M_{\rm A}\,, \tag{A.1}$$

while evaluation in the πA c.m.s. yields

$$s = (\omega_{\rm c.m.} + E_{\rm c.m.})^2 = m_\pi^2 + M_{\rm A}^2 + 2k_{\rm c.m.}^2 + 2\sqrt{(k_{\rm c.m.}^2 + m_\pi^2)(k_{\rm c.m.}^2 + M_{\rm A}^2)}\,, \tag{A.2}$$

where $k_{\rm c.m.}$ is the πA c.m. momentum and $\omega_{\rm c.m.} = \sqrt{k_{\rm c.m.}^2 + m_\pi^2}$. Equating (A.1) and (A.2), the standard relation

$$k_{\rm c.m.} = \frac{M_{\rm A}}{\sqrt{s}} k \tag{A.3}$$

results. Hence, the following relations are obtained for $k_{\pi d}$ and $k_{\pi N}$, the πd and πN c.m. momenta, respectively:

$$k_{\pi d} = [M_D/\sqrt{m_\pi^2 + M_D^2 + 2\omega M_D}]k\,, \tag{A.4}$$

$$k_{\pi N} = [M_N/\sqrt{m_\pi^2 + M_N^2 + 2\omega M_N}]k\,, \tag{A.5}$$

where $M_D = 2M_N - B_D$ is the deuteron mass (B_D is the deuteron binding energy).

Appendix B

EVALUATION OF MATRIX ELEMENTS

In this appendix the matrix elements defined by eqs. (3.1), (3.7), (3.8) and (3.25), which are required for the evaluation of the πd disintegration cross section, are discussed in some detail. For the sake of simplicity, we omit the vertex form factors in the rescattering terms and replace the $2\pi(1^-)$ contribution to p-wave rescattering by a zero-width ρ-meson exchange. Neither simplification significantly affects the generality of the development. Inclusion of vertex form factors, after performing some partial fraction separations, just introduces additional terms of the same form as those considered; while incorporation of the full two-pion mass distribution merely complicates the notation. Although not discussed here, both the form factors and the two-pion mass distribution have been included in the numerical computations.

The IA term without recoil corrections, the p-wave rescattering term, and the s-wave rescattering term can all be treated together using the same formalism. The recoil terms, on the other hand, require a separate discussion due to the derivative operators present. For this reason we first develop the formalism with recoil terms excluded and afterwards indicate how these terms may be incorporated.

B.1. MATRIX ELEMENTS WITHOUT RECOIL TERMS

We begin by evaluating the isospin matrix elements. Since both the deuteron and the outgoing pp state are states of definite isospin, only one set of matrix elements is relevant: that with $T = 0$ in the initial state and $T = 1$ in the final state. To obtain these, we note that

$$\langle T=1|\sqrt{2}\tau_{2+}|T=0\rangle = -\langle T=1|\sqrt{2}\tau_{1+}|T=0\rangle = 1\,, \tag{B.1}$$

$$\langle T=1|\sqrt{2}(\boldsymbol{\tau}_1 \times \boldsymbol{\tau}_2)|T=0\rangle = 2i\,, \tag{B.2}$$

$$\langle T=1|(\boldsymbol{T}_1 \cdot \boldsymbol{\tau}_2)T_{1+}^+|T=0\rangle = -\langle T=1|(\boldsymbol{\tau}_1 \cdot \boldsymbol{T}_2)T_{2+}^+|T=0\rangle\,,$$

$$= \tfrac{4}{3}\,, \tag{B.3}$$

where τ_i and T_i are the ordinary and transition isospin operators acting on nucleon i. The first two relations yield

$$\langle T=1|\hat{M}_{\mathrm{IA}}|T=0\rangle=\frac{f}{m_\pi}[\mathrm{e}^{i\boldsymbol{k}\cdot\boldsymbol{r}/2}(\boldsymbol{\sigma}_1\cdot\boldsymbol{k})-\mathrm{e}^{-i\boldsymbol{k}\cdot\boldsymbol{r}/2}(\boldsymbol{\sigma}_2\cdot\boldsymbol{k})], \tag{B.4}$$

$$\langle T=1|\hat{M}_{\mathrm{S}}|T=0\rangle=-2i\frac{f}{m_\pi}\left(\frac{\mu}{m_\pi}\right)\left[\lambda_1+(\omega+q_0)\frac{\lambda_2}{m_\pi}\right]Y_1(\mu r)$$
$$\times[\mathrm{e}^{i\boldsymbol{k}\cdot\boldsymbol{r}/2}(\boldsymbol{\sigma}_2\cdot\hat{\boldsymbol{r}})+\mathrm{e}^{-i\boldsymbol{k}\cdot\boldsymbol{r}/2}(\boldsymbol{\sigma}_1\cdot\hat{\boldsymbol{r}})] \tag{B.5}$$

for the IA and s-wave rescattering matrix elements, where

$$Y_1(ar)\equiv\left(1+\frac{1}{ar}\right)\frac{\mathrm{e}^{-ar}}{r}, \tag{B.6}$$

and all other quantities are defined as in sect. 3. Using the third relation, eq. (B.3), we obtain for the combined contribution of π- and ρ-exchange to the p-wave rescattering matrix element

$$\langle T=1|\hat{M}_{\mathrm{P}}|T=0\rangle=\frac{f^*_{\mathrm{eff}}}{m_\pi}D_\Delta(k_{\pi\mathrm{N}},s)\{\mathrm{e}^{i\boldsymbol{k}\cdot\boldsymbol{r}/2}[F_\sigma(r)(\boldsymbol{S}_1\cdot\boldsymbol{\sigma}_2)+F_{\mathrm{T}}(r)S^*_{12}(\hat{\boldsymbol{r}})](\boldsymbol{S}_1^+\cdot\boldsymbol{k}_{\pi\mathrm{N}})$$
$$-\mathrm{e}^{-i\boldsymbol{k}\cdot\boldsymbol{r}/2}[F_\sigma(r)(\boldsymbol{\sigma}_1\cdot\boldsymbol{S}_2)+F_{\mathrm{T}}(r)S^*_{21}(\hat{\boldsymbol{r}})](\boldsymbol{S}_2^+\cdot\boldsymbol{k}_{\pi\mathrm{N}})\}. \tag{B.7}$$

Here we have introduced the notation

$$F_\sigma(r)\equiv\frac{1}{9\pi}\left[ff^*\left(\frac{\mu}{m_\pi}\right)^2Y_0(\mu r)+2f_\rho f^*_\rho Y_0(m_\rho r)\right],$$

$$F_{\mathrm{T}}(r)\equiv\frac{1}{9\pi}\left[ff^*\left(\frac{\mu}{m_\pi}\right)^2Y_2(\mu r)-f_\rho f^*_\rho Y_2(m_\rho r)\right], \tag{B.8}$$

with

$$Y_0(ar)\equiv\mathrm{e}^{-ar}/r, \tag{B.9}$$

$$Y_2(ar)\equiv\left(1+\frac{3}{ar}+\frac{3}{(ar)^2}\right)\mathrm{e}^{-ar}/r, \tag{B.10}$$

and $f^*_\rho=\alpha_\rho f_\rho$. The Δ_{33} propagator D_Δ and the NΔ transition tensor operator S^*_{12} are given by eqs. (3.9) and (3.16) in sect. 3.

For what follows, it is convenient to combine the two terms multiplied by different exponential factors in each of eqs. (B.4), (B.5) and (B.7) by projecting out the spin singlet and spin triplet contributions to the matrix elements using the appropriate projection operators. These are given by

$$\hat{P}_{\mathrm{S}}=\tfrac{1}{4}[1-(\boldsymbol{\sigma}_1\cdot\boldsymbol{\sigma}_2)];\qquad\hat{P}_{\mathrm{T}}=\tfrac{1}{4}[3+(\boldsymbol{\sigma}_1\cdot\boldsymbol{\sigma}_2)], \tag{B.11}$$

and satisfy

$$\hat{P}_i\hat{P}_j=\hat{P}_i\delta_{ij}, \tag{B.12}$$

where $i, j = S, T$. Since the deuteron is a state of definite spin $S = 1$, we need only consider matrix element projections of the form

$$\begin{aligned}\langle M\rangle_S &\equiv \hat{P}_S\langle T=1|M|T=0\rangle\hat{P}_T\,,\\ \langle M\rangle_T &\equiv \hat{P}_T\langle T=1|M|T=0\rangle\hat{P}_T\,.\end{aligned} \tag{B.13}$$

For the IA and s-wave rescattering terms, the relations

$$\begin{aligned}\hat{P}_S\boldsymbol{\sigma}_1\hat{P}_T &= -\hat{P}_S\boldsymbol{\sigma}_2\hat{P}_T\,,\\ \hat{P}_T\boldsymbol{\sigma}_1\hat{P}_T &= \hat{P}_T\boldsymbol{\sigma}_2\hat{P}_T\end{aligned} \tag{B.14}$$

yield

$$\begin{aligned}\langle M_{IA}\rangle_S &= -\frac{f}{m_\pi}(e^{i\boldsymbol{k}\cdot\boldsymbol{r}/2}+e^{-i\boldsymbol{k}\cdot\boldsymbol{r}/2})\hat{P}_S(\boldsymbol{\sigma}_2\cdot\boldsymbol{k})\hat{P}_T\,,\\ \langle M_{IA}\rangle_T &= \frac{f}{m_\pi}(e^{i\boldsymbol{k}\cdot\boldsymbol{r}/2}-e^{-i\boldsymbol{k}\cdot\boldsymbol{r}/2})\hat{P}_T(\boldsymbol{\sigma}_2\cdot\boldsymbol{k})\hat{P}_T\,,\\ \langle M_s\rangle_S &= -i\frac{f}{m_\pi}\mathcal{S}(r)(e^{i\boldsymbol{k}\cdot\boldsymbol{r}/2}-e^{-i\boldsymbol{k}\cdot\boldsymbol{r}/2})\hat{P}_S(\boldsymbol{\sigma}_2\cdot\hat{\boldsymbol{r}})\hat{P}_T\,,\\ \langle M_s\rangle_T &= -i\frac{f}{m_\pi}\mathcal{S}(r)(e^{i\boldsymbol{k}\cdot\boldsymbol{r}/2}+e^{-i\boldsymbol{k}\cdot\boldsymbol{r}/2})\hat{P}_T(\boldsymbol{\sigma}_2\cdot\hat{\boldsymbol{r}})\hat{P}_T\,,\end{aligned} \tag{B.15}$$

with the abbreviation

$$\mathcal{S}(r)\equiv\frac{\mu}{m_\pi}2\left[\lambda_1+(\omega+q_0)\frac{\lambda_2}{m_\pi}\right]Y_1(\mu r)\,. \tag{B.17}$$

To obtain the corresponding projections of the p-wave rescattering matrix element, we note that

$$\begin{aligned}(\boldsymbol{S}_1\cdot\boldsymbol{\sigma}_2)(\boldsymbol{S}_1^+\cdot\boldsymbol{k}_{\pi N}) &= \boldsymbol{\sigma}_2\cdot\boldsymbol{k}_{\pi N}-\tfrac{1}{3}(\boldsymbol{\sigma}_1\cdot\boldsymbol{\sigma}_2)(\boldsymbol{\sigma}_1\cdot\boldsymbol{k}_{\pi N})\\ &= \boldsymbol{\sigma}_2\cdot\boldsymbol{k}_{\pi N}+\hat{P}_S(\boldsymbol{\sigma}_1\cdot\boldsymbol{k}_{\pi N})-\tfrac{1}{3}\hat{P}_T(\boldsymbol{\sigma}_1\cdot\boldsymbol{k}_{\pi N})\,,\end{aligned} \tag{B.18}$$

$$S_{12}^*(\hat{\boldsymbol{r}})(\boldsymbol{S}_1^+\cdot\boldsymbol{k}_{\pi N}) = 3(\boldsymbol{\sigma}_2\cdot\hat{\boldsymbol{r}})(\boldsymbol{k}_{\pi N}\cdot\hat{\boldsymbol{r}})-\boldsymbol{\sigma}_2\cdot\boldsymbol{k}_{\pi N}-\tfrac{1}{3}S_{12}(\hat{\boldsymbol{r}})(\boldsymbol{\sigma}_1\cdot\boldsymbol{k}_{\pi N})\,. \tag{B.19}$$

Here S_{12} is the ordinary tensor operator, defined by

$$S_{12}(\hat{\boldsymbol{r}})\equiv 3(\boldsymbol{\sigma}_1\cdot\hat{\boldsymbol{r}})(\boldsymbol{\sigma}_2\cdot\hat{\boldsymbol{r}})-\boldsymbol{\sigma}_1\cdot\boldsymbol{\sigma}_2\,, \tag{B.20}$$

and with spin projections

$$\hat{P}_S S_{12}=0\,,\qquad \hat{P}_T S_{12}=S_{12}\,. \tag{B.21}$$

Thus,

$$\langle M_{\rm P}\rangle_{\rm S}=\frac{f^*_{\rm eff}}{m_\pi}D_\Delta(k_{\pi\rm N},s)(e^{i\boldsymbol{k}\cdot\boldsymbol{r}/2}+e^{i\boldsymbol{k}\cdot\boldsymbol{r}/2})F_{\rm T}(r)\hat{P}_{\rm S}[3(\boldsymbol{\sigma}_2\cdot\hat{\boldsymbol{r}})(\boldsymbol{k}_{\pi\rm N}\cdot\hat{\boldsymbol{r}})-\boldsymbol{\sigma}_2\cdot\boldsymbol{k}_{\pi\rm N}]\hat{P}_{\rm T}\,,$$

$$\langle M_{\rm P}\rangle_{\rm T}=\frac{f^*_{\rm eff}}{m_\pi}D_\Delta(k_{\pi\rm N},s)(e^{i\boldsymbol{k}\cdot\boldsymbol{r}/2}-e^{i\boldsymbol{k}\cdot\boldsymbol{r}/2})\{\tfrac{2}{3}F_\sigma(r)\hat{P}_{\rm T}(\boldsymbol{\sigma}_2\cdot\boldsymbol{k}_{\pi\rm N})\hat{P}_{\rm T}\,,$$

$$+F_{\rm T}(r)\hat{P}_{\rm T}[3(\boldsymbol{\sigma}_2\cdot\hat{\boldsymbol{r}})(\boldsymbol{k}_{\pi\rm N}\cdot\hat{\boldsymbol{r}})-\boldsymbol{\sigma}_2\cdot\boldsymbol{k}_{\pi\rm N}-\tfrac{1}{3}S_{12}(\hat{\boldsymbol{r}})(\boldsymbol{\sigma}_2\cdot\boldsymbol{k}_{\pi\rm N})]\hat{P}_{\rm T}\}\,. \tag{B.22}$$

We must now specify explicitly the initial- and final-state nucleon wave functions. The initial deuteron state is just a superposition of $^3S_1$ and $^3D_1$ wave functions:

$$|i\rangle=\frac{u(r)}{r}|(10)1M_{\rm d}\rangle+\frac{w(r)}{r}|(12)1M_{\rm d}\rangle\,. \tag{B.23}$$

Here u and w are the s- and d-state radial wave functions, $M_{\rm d}$ is the total angular momentum projection in the initial state, and

$$|(1l_{\rm d})1M_{\rm d}\rangle\equiv\sum_{M_{\rm S}}(1M_{\rm S}l_{\rm d}M_{\rm d}-M_{\rm S}|1M_{\rm d})\chi_{1M_{\rm S}}Y_{l_{\rm d}M_{\rm d}-M_{\rm S}}(\Omega)\,, \tag{B.24}$$

with χ and Y denoting spin-1 wave functions and spherical harmonics respectively. The outgoing pp wave function in a particular spin state can be cast in the form

$$\langle{\rm f}|=4\pi\sum_{lM_l}(-i)^lY_{lM_l}(\hat{\boldsymbol{p}})\sum_{JM_J}(SM_Sl M_l|JM_J)u_{lJ}(r)\langle[(Sl)JM_J|\,, \tag{B.25}$$

where S, l, and J are the spin, orbital and total angular momentum, p is the relative pp momentum, and u_{lJ} is the radial wave function. In the absence of pp correlations, u_{lJ} reduces to the spherical Bessel function $j_l(pr)$, and eq. (B.25) becomes just the partial wave expansion of a plane wave coupled to a spin wave function.

The next step is to combine the final-state nucleon wave function given above with the exponential factors appearing in the spin-projected matrix elements. We accomplish this by first expanding the exponential factors in partial waves and then coupling the expressions so obtained to the partial wave expansion, eq. (B.25), using the addition theorem for spherical harmonics. The result, with the quantization axis fixed along the direction of $\boldsymbol{k}$, is

$$\langle{\rm f}|(e^{i\boldsymbol{k}\cdot\boldsymbol{r}/2}\pm e^{-i\boldsymbol{k}\cdot\boldsymbol{r}/2})=2(4\pi)^{3/2}\sum_{l_\pi\,\text{odd}}^{\text{even}}i^{l_\pi}(2l_\pi+1)^{1/2}j_{l_\pi}(\tfrac{1}{2}kr)$$

$$\times\sum_{lM_l}(-i)^lY_{lM_l}(\hat{\boldsymbol{p}})\sum_{JM_J}(SM_Sl M_l|JM_J)u_{lJ}(r)$$

$$\times\sum_{J_t}(JM_Jl_\pi 0|J_tM_J)\langle[(Sl)Jl_\pi]J_tM_J|\,, \tag{B.26}$$

where J_f is the total angular momentum of the final state plus incoming pion, and the choice even or odd in the sum over l_π is governed by the sign between the exponentials on the l.h.s. This expansion is relatively simple but employs an angular momentum coupling scheme inconvenient for evaluation of the matrix elements. A more useful expansion can be obtained by recoupling the angular momenta so that S is coupled to the total orbital angular momentum $\boldsymbol{L} = \boldsymbol{l} + \boldsymbol{l}_\pi$, rather than to l alone. The appropriate transformation is given by

$$\langle[(Sl)Jl_\pi]J_fM_J| = (4\pi)^{-1/2}(-)^{S+J_f}\hat{l}\hat{l}_\pi\hat{J} \times \sum_L \hat{L}\begin{pmatrix} l & l_\pi & L \\ 0 & 0 & 0 \end{pmatrix}\begin{Bmatrix} L & J_f & S \\ J & l & l_\pi \end{Bmatrix}\langle[S(ll_\pi)L]J_fM_J|\,, \tag{B.27}$$

with the notation

$$\hat{l}_i = (2l_i + 1)^{1/2} \tag{B.28}$$

From the form of eq. (B.27) and the spin-projected isospin matrix elements, it is clear that matrix elements of the type $\langle[S(ll_\pi)L]J_fM_J|\theta|(1l_d)1M_d\rangle$, where θ is one of the angular momentum operators appearing in eqs. (B.15) and (B.22), need to be considered. We evaluate such matrix elements using standard procedures. For the operators $\boldsymbol{\sigma}_2 \cdot \boldsymbol{k}$, $\boldsymbol{\sigma}_2 \cdot \hat{\boldsymbol{r}}$, and $3(\boldsymbol{\sigma}_2 \cdot \hat{\mathbf{r}})(\mathbf{k}_{\pi N} \cdot \hat{\boldsymbol{r}}) - \boldsymbol{\sigma}_2 \cdot \boldsymbol{k}_{\pi N}$ we then obtain

$$\langle[S(ll_\pi)L]J_fM_J|\boldsymbol{\sigma}_2 \cdot \boldsymbol{k}|(1l_d)1M_d\rangle = (-)^{J_f+M_d+S}\sqrt{3}k\delta_{M_JM_d}\delta_{Ll_d}\hat{J}_f\begin{pmatrix} 1 & 1 & J_f \\ 0 & M_d & -M_d \end{pmatrix}\begin{Bmatrix} 1 & S & 1 \\ J_f & 1 & l_d \end{Bmatrix}\langle S\|\boldsymbol{\sigma}_2\|1\rangle\,, \tag{B.29}$$

$$\langle[S(ll_\pi)L]J_fM_J|\boldsymbol{\sigma}_2 \cdot \hat{\boldsymbol{r}}|(1l_d)1M_d\rangle = \delta_{M_JM_d}\delta_{J_f1}\hat{L}\hat{l}_d\begin{pmatrix} 1 & l_d & L \\ 0 & 0 & 0 \end{pmatrix}\begin{Bmatrix} 1 & L & S \\ 1 & 1 & l_d \end{Bmatrix}\langle S\|\boldsymbol{\sigma}_2\|1\rangle\,, \tag{B.30}$$

$$\langle[S(ll_\pi)L]J_fM_J|3(\boldsymbol{\sigma}_2 \cdot \hat{\boldsymbol{r}})(\boldsymbol{k}_{\pi N} \cdot \hat{\boldsymbol{r}}) - \boldsymbol{\sigma}_2 \cdot \boldsymbol{k}_{\pi N}|(1l_d)1M_d\rangle = (-)^{J_f+M_d+1}3\sqrt{10}k_{\pi N}\delta_{M_JM_d}\hat{J}_f\hat{L}\hat{l}_d\begin{pmatrix} 1 & 1 & J_f \\ 0 & M_d & -M_d \end{pmatrix}\begin{pmatrix} 2 & l_d & L \\ 0 & 0 & 0 \end{pmatrix} \times \begin{Bmatrix} S & 1 & 1 \\ L & l_d & 2 \\ J_f & 1 & 1 \end{Bmatrix}\langle S\|\boldsymbol{\sigma}_2\|1\rangle\,, \tag{B.31}$$

with

$$\langle S\|\boldsymbol{\sigma}_2\|1\rangle = \sqrt{3}\delta_{S0} + \sqrt{6}\delta_{S1} \tag{B.32}$$

for the reduced spin matrix element. The operator $S_{12}(\hat{\boldsymbol{r}})(\boldsymbol{\sigma}_2 \cdot \boldsymbol{k}_{\pi N})$ is not expressible as a single product of tensor operators and hence, is more complicated than the others, but it can still be treated within the same procedure. After some lengthy

angular momentum algebra, a relatively simple expression results for the matrix element:

$$\langle [S(ll_\pi)L]J_fM_J|S_{12}(\hat{\boldsymbol{r}})(\boldsymbol{\sigma}_2\cdot\boldsymbol{k}_{\pi N})|(1l_d)1M_d\rangle$$
$$=(-)^{M_J}12\sqrt{15}k_{\pi N}\delta_{M_JM_d}\delta_{S1}\hat{J}_f\hat{l}_d\hat{L}\begin{pmatrix}1 & 1 & J_f\\ 0 & M_d & -M_d\end{pmatrix}\begin{pmatrix}2 & l_d & L\\ 0 & 0 & 0\end{pmatrix}$$
$$\times\begin{Bmatrix}l_d & J_f & 1\\ 1 & 1 & 1\end{Bmatrix}\begin{Bmatrix}l_d & L & 2\\ 1 & 1 & J_f\end{Bmatrix}. \tag{B.33}$$

We can now assemble the complete matrix elements from the isospin matrix elements, eqs. (B.15) and (B.22), the wave functions, eqs. (B.23), (B.26) and (B.27), and the angular momentum matrix elements, eqs. (B.29)–(B.31) and (B.33). The resulting expressions are as follows:

$$\langle f|M_{IA+p}|i\rangle_{S=0}=8\pi\sum_{l\,\text{even}}\hat{l}Y_{lM_d}(\hat{\boldsymbol{p}})$$
$$\times\Big[\delta_{M_d0}\mathscr{F}_l-(-)^{l/2}\begin{pmatrix}1 & 1 & 2\\ 0 & M_d & -M_d\end{pmatrix}\sum_{l_\pi\,\text{even}}(-)^{l_\pi/2}(2l_\pi+1)$$
$$\times\begin{pmatrix}l & l_\pi & 2\\ 0 & 0 & 0\end{pmatrix}\begin{pmatrix}l & l_\pi & 2\\ M_d & 0 & -M_d\end{pmatrix}\mathscr{F}_{ll_\pi}\Big], \tag{B.34}$$

$$\langle f|M_{IA+p}|i\rangle_{S=1}=8\pi\sum_{l\,\text{odd}}\hat{l}Y_{l(M_d-M_s)}(\hat{\boldsymbol{p}})\sum_J(2J+1)\begin{pmatrix}1 & l & J\\ M_s & M_d-M_s & -M_d\end{pmatrix}$$
$$\times\Big[(-)^J\delta_{M_d,\pm1}\begin{pmatrix}1 & 1 & 1\\ 0 & M_d & -M_d\end{pmatrix}\begin{pmatrix}l & 1 & J\\ 0 & M_d & -M_d\end{pmatrix}D_0^{lJ}$$
$$+(-)^{M_d+l/2}\sum_{l_\pi\,\text{odd}}(-)^{l\pi/2}(2l_\pi+1)\begin{pmatrix}l & l_\pi & 2\\ 0 & 0 & 0\end{pmatrix}$$
$$\times\sum_{J_f=1,2}\begin{pmatrix}1 & J_f & 1\\ 0 & M_d & -M_d\end{pmatrix}\begin{pmatrix}l_\pi & J_f & J\\ 0 & M_d & -M_d\end{pmatrix}\begin{Bmatrix}l_\pi & l & 2\\ 1 & J_f & J\end{Bmatrix}D_{J_f}^{l_\pi lJ}\Big], \tag{B.35}$$

$$\langle f|M_S|i\rangle_{S=0}=8\pi\sum_{l\,\text{even}}(-)^{M_d+l/2}\hat{l}Y_{lM_d}(\hat{\boldsymbol{p}})$$
$$\times\sum_{l_\pi\,\text{odd}}(-)^{(l_\pi+1)/2}(2l_\pi+1)\begin{pmatrix}l & l_\pi & 1\\ 0 & 0 & 0\end{pmatrix}\begin{pmatrix}l & l_\pi & 1\\ M_d & 0 & -M_d\end{pmatrix}$$
$$\times(R_S^{l_\pi l10}-\sqrt{2}R_S^{l_\pi l12}), \tag{B.36}$$

$$\langle \mathrm{f}|M_s|\mathrm{i}\rangle_{S=1} = 8\pi \sum_{l\ \mathrm{odd}} (-)^{(l+1)/2}\hat{l}Y_{lM_d-M_s}(\hat{\boldsymbol{p}}) \sum_J (-)^J(2J+1)$$
$$\times \begin{pmatrix} 1 & l & J \\ M_s & M_d-M_s & -M_d \end{pmatrix} \sum_{l_\pi\ \mathrm{even}} (-)^{l_\pi/2}(2l_\pi+1) \begin{pmatrix} l & l_\pi & 1 \\ 0 & 0 & 0 \end{pmatrix}$$
$$\times \begin{pmatrix} J & l_\pi & 1 \\ M_d & 0 & -M_d \end{pmatrix} \begin{Bmatrix} 1 & 1 & 1 \\ J & l & l_\pi \end{Bmatrix} (\sqrt{6}R_S^{l_\pi lJ0} + \sqrt{3}R_S^{l_\pi lJ2}), \qquad \text{(B.37)}$$

where

$$\mathscr{F}_l \equiv R_{\mathrm{IA}}^{llJ0} + \sqrt{\tfrac{1}{2}}R_{\mathrm{T}}^{llJ2},$$
$$\mathscr{F}_{ll_\pi} \equiv \sqrt{15}(R_{\mathrm{IA}}^{l_\pi lJ0} + \sqrt{\tfrac{1}{2}}R_{\mathrm{T}}^{l_\pi lJ0} + \tfrac{1}{2}R_{\mathrm{T}}^{l_\pi lJ2}), \qquad \text{(B.38)}$$
$$D_0^{lJ} \equiv \sqrt{6}(R_{\mathrm{IA}}^{llJ0} + R_\sigma^{llJ0} + \tfrac{5}{12}\sqrt{2}R_{\mathrm{T}}^{llJ2}),$$
$$D_1^{l_\pi lJ} \equiv \sqrt{10}[\tfrac{3}{2}(R_{\mathrm{IA}}^{l_\pi lJ2} + R_\sigma^{l_\pi lJ2}) + \tfrac{1}{4}\sqrt{2}R_{\mathrm{T}}^{l_\pi lJ0} - R_{\mathrm{T}}^{l_\pi lJ2}],$$
$$D_2^{l_\pi lJ} \equiv \tfrac{5}{2}\sqrt{2}[3(R_{\mathrm{IA}}^{l_\pi lJ2} + R_\sigma^{l_\pi lJ2}) + \tfrac{3}{2}\sqrt{2}R_{\mathrm{T}}^{l_\pi lJ0} - R_{\mathrm{T}}^{l_\pi lJ2}], \qquad \text{(B.39)}$$

and the radial integrals are defined by

$$R_{\mathrm{IA}}^{l_\pi lJl_{\mathrm{d}}} \equiv \left(\frac{f}{m_\pi}\right) k \int r^2\,\mathrm{d}r\, j_{l_\pi}(\tfrac{1}{2}kr)u_{lJ}(r)\varphi_{l_{\mathrm{d}}}(r),$$
$$R_\sigma^{l_\pi lJl_{\mathrm{d}}} \equiv \frac{2}{3}\left(\frac{f_{\mathrm{eff}}^*}{m_\pi}\right) k_{\pi\mathrm{N}} D_\Delta \int r^2\,\mathrm{d}r\, j_{l_\pi}(\tfrac{1}{2}kr)u_{lJ}(r)F_\sigma(r)\varphi_{l_{\mathrm{d}}}(r),$$
$$R_{\mathrm{T}}^{l_\pi lJl_{\mathrm{d}}} \equiv 2\left(\frac{f_{\mathrm{eff}}^*}{m_\pi}\right) k_{\pi\mathrm{N}} D_\Delta \int r^2\,\mathrm{d}r\, j_{l_\pi}(\tfrac{1}{2}kr)u_{lJ}(r)F_{\mathrm{T}}(r)\varphi_{l_{\mathrm{d}}}(r),$$
$$R_S^{l_\pi lJl_{\mathrm{d}}} \equiv \left(\frac{f}{m_\pi}\right) \int r^2\,\mathrm{d}r\, j_{l_\pi}(\tfrac{1}{2}kr)u_{lJ}(r)\mathscr{S}(r)\varphi_{l_{\mathrm{d}}}(r), \qquad \text{(B.40)}$$

with $\varphi_0(r) \equiv u(r)/r$ and $\varphi_2(r) \equiv w(r)/r$. Note in these expressions that we have combined the IA and p-wave rescattering matrix elements and performed the sums over J_{f}, L, and l_{d}.

B.2. RECOIL TERMS

The recoil terms require a slightly modified treatment due to the derivative operators that they contain. In particular, since these derivatives act only on the relative outgoing pp state when final-state correlations are neglected, it is convenient for evaluation of the recoil matrix elements, to couple the pion wave function to the initial deuteron state rather than to the final pp state. Thus, instead of eqs. (B.23),

(B.26) and (B.27), we employ

$$(e^{i\mathbf{k}\cdot\mathbf{r}/2}\pm e^{-i\mathbf{k}\cdot\mathbf{r}/2})|i\rangle = 2\sum_{\substack{l_\pi \text{even}\\ l_\pi \text{odd}}} i^{l_\pi}(2l_\pi+1)j_{l_\pi}(\tfrac{1}{2}kr)$$
$$\times\sum_{l_d=0,2}\hat{l}_d\varphi_{l_d}(r)\sum_{M_T}(1M_T l_d M_d - M_T|1M_d)\sum_{LJ_i}\hat{L}\begin{pmatrix} l_\pi & l_d & L\\ 0 & 0 & 0\end{pmatrix}$$
$$\times\begin{pmatrix} l_\pi & l_d & L\\ 0 & M_d-M_T & M_T-M_d\end{pmatrix}(J_iM_d|1M_TLM_d-M_T)|[1(l_\pi l_d)L]J_iM_d\rangle\,, \qquad \text{(B.41)}$$

and eq. (B.25) without correlations to represent the initial- and final-state wave functions respectively. Note in the above that $\boldsymbol{L}=\boldsymbol{l}_\pi+\boldsymbol{l}_d$, M_T is the deuteron spin projection, and J_i is the total angular momentum of the initial deuteron plus incoming pion.

The spin-projected isospin matrix elements for the recoil terms can be obtained in the same manner as before with the results

$$\langle M_r\rangle_S = i\left(\frac{f}{m_\pi}\right)\beta\frac{\omega}{M}(e^{i\mathbf{k}\cdot\mathbf{r}/2}-e^{i\mathbf{k}\cdot\mathbf{r}/2})\hat{P}_S(\boldsymbol{\sigma}_2\cdot\boldsymbol{\nabla}\hat{P}_T\,,$$
$$\langle M_r\rangle_T = -i\left(\frac{f}{m_\pi}\right)\beta\frac{\omega}{M}(e^{i\mathbf{k}\cdot\mathbf{r}/2}+e^{i\mathbf{k}\cdot\mathbf{r}/2})\hat{P}_T\boldsymbol{\sigma}_2\cdot\boldsymbol{\nabla}\hat{P}_T\,, \qquad \text{(B.42)}$$

where ∇ acts only on the relative outgoing wave function. From these expressions and eqs. (B.25) and (B.41) for the wave functions, it is clear that the relevant angular momentum matrix element is $\langle(Sl)JM_J|\boldsymbol{\sigma}_2\cdot\nabla|[1(l_\pi l_d)L]J_iM_d\rangle$. To evaluate this matrix element, we again proceed as before. This yields

$$\langle(Sl)JM_J|\boldsymbol{\sigma}_2\cdot\nabla|[1(l_\pi l_d)L]J_iM_d\rangle = (-)^{l+J+1}\delta_{M_JM_d}\delta_{JJ_i}\begin{Bmatrix} J & l & S\\ 1 & 1 & L\end{Bmatrix}\langle S\|\boldsymbol{\sigma}_2\|1\rangle\langle l\|\nabla\|L\rangle\,, \qquad \text{(B.43)}$$

with eq. (B.32) and

$$\langle l\|\nabla\|L\rangle = \delta_{L,l-1}l^{1/2}\left(\frac{\partial}{\partial r}+\frac{l+1}{r}\right)-\delta_{L,l+1}(l+1)^{1/2}\left(\frac{\partial}{\partial r}-\frac{l}{r}\right) \qquad \text{(B.44)}$$

for the reduced matrix elements, where the derivatives act on the outgoing spherical Bessel function, $j_l(pr)$. Finally, combining eqs. (B.25), (B.42) and (B.43) and performing the sums over J_i and l_d, we obtain the complete recoil matrix elements:

$$\langle f|M_r|i\rangle_{S=0} = 8\pi\sum_{l\,\text{even}}(-)^{l/2}Y_{lM_d}(\hat{\boldsymbol{p}})\sum_{l_\pi\,\text{odd}}(-)^{(l_\pi+1)/2}$$
$$\times\left[\begin{pmatrix} l & l_\pi & 1\\ M_d & 0 & -M_d\end{pmatrix}\mathcal{R}_{l_\pi}^{l_\pi l0}-(-)^{M_d}(2l_\pi+1)\sum_{L\,\text{odd},\,M_T}\Theta_{M_T,L}\right.$$
$$\left.\times\begin{pmatrix} l & L & 1\\ M_d & M_T-M_d & -M_T\end{pmatrix}\mathcal{R}_L^{l_\pi l2}\right], \qquad \text{(B.45)}$$

$$\langle f|M_r|i\rangle_{S=1} = 8\pi \sum_{l\,\text{odd}} (-)^{(l+1)/2} Y_{lM_d-M_S}(\hat{\boldsymbol{p}}) \sum_{l_\pi\,\text{even}} (-)^{l_\pi/2}$$

$$\times \sum_J (-)^J (2J+1) \begin{pmatrix} 1 & l & J \\ M_S & M_d - M_S & -M_d \end{pmatrix} \sqrt{6} \Bigg[(-)^{M_d} \begin{pmatrix} J & l_\pi & 1 \\ M_d & 0 & -M_d \end{pmatrix}$$

$$\times \begin{Bmatrix} J & l & 1 \\ 1 & 1 & l_\pi \end{Bmatrix} \mathcal{R}_{l_\pi}^{l_\pi l 0} - (2l_\pi + 1) \sum_{L\,\text{even},\, M_T} \Theta_{M_T,L} \begin{pmatrix} J & L & 1 \\ M_d & M_T - M_d & -M_T \end{pmatrix}$$

$$\times \begin{Bmatrix} J & l & 1 \\ 1 & 1 & L \end{Bmatrix} \mathcal{R}_L^{L l 2} \Bigg], \tag{B.46}$$

with

$$\Theta_{M_T,L} \equiv (-)^{M_T} \sqrt{15} \begin{pmatrix} 1 & 2 & 1 \\ M_T & M_d - M_T & -M_d \end{pmatrix} \begin{pmatrix} l_\pi & L & 2 \\ 0 & 0 & 0 \end{pmatrix} \begin{pmatrix} l_\pi & L & 2 \\ 0 & M_T - M_d & M_d - M_T \end{pmatrix} \tag{B.47}$$

$$\mathcal{R}_L^{l_\pi l l_d} \equiv \sqrt{(2l+3)(l+1)}\,\delta_{L,l+1} R_+^{l\pi l l_d} - \sqrt{(2l-1)l}\,\delta_{L,l-1} R_-^{l\pi l l_d}, \tag{B.48}$$

where

$$R_+^{l_\pi l l_d} \equiv \left(\frac{f}{m_\pi}\right) \beta\left(\frac{\omega}{M}\right) \int r^2\, \mathrm{d}r\, j_{l_\pi}(\tfrac{1}{2}kr) \varphi_{l_d}(r) \left(\frac{\partial}{\partial r} - \frac{l}{r}\right) j_l(pr),$$

$$R_-^{l_\pi l l_d} \equiv \left(\frac{f}{m_\pi}\right) \beta\left(\frac{\omega}{M}\right) \int r^2\, \mathrm{d}r\, j_{l_\pi}(\tfrac{1}{2}kr) \varphi_{l_d}(r) \left(\frac{\partial}{\partial r} + \frac{l+1}{r}\right) j_l(pr). \tag{B.49}$$

References

1) C.M. Ko and D.O. Riska, Nucl. Phys. **A312** (1978) 217;
J. Chai and D.O. Riska, Nucl. Phys. **A329** (1979) 429
2) E. Oset and W. Weise, Nucl. Phys. **A319** (1979) 477; **A329** (1979) 365;
E. Oset, W. Weise and R. Brockmann, Phys. Lett. **82B** (1979) 344
3) A.M. Green and M.E. Sainio, Nucl. Phys. **A329** (1979) 477;
K. Shimizu and A. Faessler, Phys. Rev. **C17** (1979) 1891; preprint (1979), to be published
4) C. Richard-Serre *et al.*, Nucl. Phys. **B20** (1970) 413
5) D. Aebischer *et al.*, Nucl. Phys. **B108** (1976) 214
6) B.M. Preedom *et al.*, Phys. Rev. **C17** (1978) 1402
7) W. Hürster *et al.*, Proc. 8th Int. Conf. on few body systems and nuclear forces, Graz (1978), Lecture notes in physics (Springer, Berlin) **82** (1978) 431; Phys. Lett. **91B** (1980) 214
H. Nann *et al.*, Northwestern Univ. preprint (1979)
8) Ch. Weddigen, Nucl. Phys. **A312** (1978) 330;
G. Jones, Proc. 8th Int. Conf. on few body systems and nuclear forces, Graz (1978), Lecture notes in physics (Springer, Berlin) **87** (1978) 142
9) P. Walden *et al.*, Phys. Lett. **81B** (1979) 156;
E. Aprile *et al.*, Univ. Geneva/SIN preprint (1979); Proc. 8th Int. Conf. on high energy physics and nuclear structure, Vancouver (1979), Nucl. Phys. **A335** (1980) 245
10) M.A. Alberg, E.M. Henley, G.A. Miller and J.F. Walker, Nucl. Phys. **A306** (1979) 447
11) J.A. Niskanen, Nucl. Phys. **A298** (1978) 417;
A.M. Green, in Mesons in nuclei, ed. M. Rho and D.H. Wilkinson, vol. I (North-Holland, Amsterdam, 1979) p. 227

12) M. Brack, D.O. Riska and W. Weise, Nucl. Phys. **A287** (1977) 425
13) D.S. Koltun and A.S. Reitan, Phys. Rev. **141** (1966) 1413
14) J. Chai and D.O. Riska, Nucl. Phys. **A338** (1980) 349
15) R.S. Bhalerao, L.C. Liu and C.M. Shakin, preprint (1979)
16) B.D. Keister and L.S. Kisslinger, Nucl. Phys **A326** (1979) 445
17) R. Vinh Mau, in Mesons in nuclei, ed. M. Rho and D.H. Wilkinson, vol. I (North-Holland, Amsterdam, 1979) p. 153;
M. Lacombe *et al.*, to be published
18) G.F. Chew and F.E. Low, Phys. Rev. **101** (1956) 1570;
G.E. Brown and W. Weise, Phys. Reports **22C** (1975) 280
19) J.W. Durso, A.D. Jackson and B.J. Verwest, Nucl. Phys. **A282** (1977) 404;
M. Dillig and M. Brack, J. Phys. **G5** (1979) 223
20) M.K. Banerjee and J.B. Cammarata, Phys. Rev. **D19** (1979) 145
21) K. Holinde, Proc. 8th Int. Conf. on few body systems and nuclear forces, Graz (1978), Lecture notes in physics (Springer, Berlin) **87** (1979) 21
22) R. Devenish, R.S. Eisenschitz and J.G. Körner, Phys. Rev. **D14** (1977) 3063
23) L.S. Kisslinger, preprint Carnegie-Mellon Univ. (1979)
24) M. Gauron, Paris preprint (1979)
25) G. Höhler and E. Pietarinen, Nucl. Phys. **B95** (1975) 210
26) J. Hamilton, High energy physics, ed. E.H.S. Burhop, vol. 1, (Academic, New York, 1967) p. 194
27) G. Höhler, R. Koch and E. Pietarinen, preprint (1978)
28) M.M. Nagels *et al.*, Nucl. Phys. **B147** (1979) 189
29) R.V. Reid, Ann. of Phys. **50** (1968) 411
30) H.J. Weber and H. Arenhövel, Phys. Reports **36C** (1978) 277
31) E. Pedroni *et al.*, Nucl. Phys. **A300** (1978) 321
32) H. Pilkuhn, Phys. Lett. **87B** (1979) 77
33) A.M. Green and J.A. Niskanen, Nucl Phys. **A271** (1976) 503
34) K. Shimizu and A. Faessler, preprint
35) O.V. Maxwell and W. Weise, Nucl. Phys. **A348** (1980) 429